Investigating APP- and β-amyloid-mediated intercellular spread of protein aggregates in a novel Drosophila Alzheimer's disease model

Adam Arous

St Hugh's College

University of Oxford

Hilary Term 2025

MSc (*by Research*) Physiology, Anatomy and Genetics

Supervisor: Professor Clive Wilson

Acknowledgements

I would first like to express my sincere gratitude to my Supervisor, Clive Wilson, for his unwavering support and guidance that has allowed me to produce this body of research. I would also like to express my gratitude to my secondary supervisor, Dr. Bhavna Verma, whose mentorship and friendship has profoundly influenced my experience throughout this project.

In addition, I would like to express my thanks to Preman Singh, whose research has both inspired both my work and furthered my passion of neuroscience. I would also like to acknowledge lab members Mark Wainwright, Amy Cording and Lewis Blincowe, who have supported me in all aspects of this project and made it such a memorable experience.

Abbreviations

AD, Alzheimer’s disease

AG, Accessory gland

APP, Amyloid precursor protein

Aβ, Amyloid-beta

DCGs, Dense core granules

CAA, Cerebral amyloid angiopathy

SCs, Secondary cells

MCs, Main Cells

ILVs. Intraluminal vesicles

EVs, Extracellular vesicle

sEV, Small extracellular vescicles

MFAS, Midline fascilin

ESCRT-III, Endosomal sorting complexes required for transport

FRT, Female reproductive tract

Pmel17, Premelanosome protein

PGRP, Peptidoglycan recognition protein

NMR, Nuclear magnetic resonance

NFTs, Neurofibrillary tangles

fAD, Familial dlzheimer’s disease

sAD, Sporadiac alzheimer’s disease

NF-κB, Nuclear factor kappa-light-chain-enhancer of activated B cells

C99, C-terminal fragment C99

δ-pathway, Delta pathway

η-pathways, Heta pathway

α-, β-, and γ-secretases, Alpha, beta and Gamma-secretases

NSCs, Neural stem cells

sAPPα, Soluble amyloid precursor protein alpha

sAPPβ, Soluble amyloid Precursor protein beta

BACE, β-site APP-cleaving enzyme 1

APLP1, Amyloid precursor like protein 1

APLP2, Amyloid precursor like protein 2

SNPs, Single nucleotide polymorphisms

PMR, Post-mating response

Rab, Ras-related protein in brain

SP, Sex peptide

SFPs, Seminal fluid proteins

TGFBI, Transforming growth factor beta induced

DAD, Daughters against DPP

DPP, Decapentaplegic

Chmp5, Charged multivesicular body protein 5

GAPDH2, Glyceraldehyde-3-phosphate dehydrogenase 2

GWAS, Genome wide association studies

PSEN1, Presenilin-1

PSEN2, Presenlin-2

Abstract

Amyloids are versatile multifaceted self-assembled nanomaterials, classified by the presence of cross-β-sheet molecular architecture. This stable conformation enables amyloids to play wide-ranging, critical physiological roles often homologous between species. However, mutations or errors in the processing and assembly of proteins with amyloidogenic potential, termed “functional amyloids”, such as amyloid precursor protein (APP), can lead to generation of toxic amyloid species, such the amyloid-beta (Aβ) peptides, which accumulates in plaques within human brain regions, where it is a central mediator of Alzheimer’s disease (AD) pathogenesis.

Our group has pioneered the use of the male accessory glands in Drosophila to model signalling functions and pathologies associated with early-stage AD. These glands contain secondary cells (SCs), a prostate-like secretory cell type within the epithelium that forms large secretory compartments that enable intra-compartmental analysis of the physiological aggregation of secretory proteins into dense-core granules (DCGs) during compartment maturation using fluorescent-microscopic analysis.

Previous work by the group has revealed that APP-like (APPL), the unique fly orthologue of human APP, is required to regulate a membrane-dependent protein aggregation priming process in these compartments. It must first be cleaved to release the APPL extracellular domain to permit formation of a large central DCG. Expressing mutant non-cleavable forms of APPL or mutant-Aβ in SCs results in defective APPL processing and DCG biogenesis, impaired lysosomal function and secretion of aggregates from these aberrant compartments. These compartments are then abnormally endocytosed by neighbouring secretory cells, called main cells (MCs) present at the glands apical tip. This induces endolysosomal defects, propagating the SC phenotype. Endolysosomal trafficking defects and intercellular propagation of pathology are implicated as fundamental and potentially initiating defects in AD pathogenesis and progression.

Herein, I have investigated the abnormal uptake phenotype using a GFP-labelled form of the protein Midline Fasciclin, MFAS, a critical component of the SC DCGs. I show that the MCs endolysosomal defects propagate throughout the accessory gland epithelium, but that it is preferentially endocytosed by subsets of MCs, generating a “mosaic like” phenotype, potentially mirroring the sub-cellular heterogeneity often demonstrated by intraneuronal-Aβ aggregates. In addition, mating experiments have enabled me to identify that different Aβ mutants have different effects on GFP-MFAS’s re-secretion from MCs during mating and its subsequent uptake, again potentially reflecting the distinct aggregation properties of these mutants.

In SCs, DCG compartments also form intra-luminal vesicles (ILVs), which are secreted as a specialised subtype of exosomes called Rab11-exosomes. These ILVs interact with DCG protein aggregates in normal SCs, and this interaction is altered in the presence of mutant APPL proteins and Aβ, which appear to stabilise membrane:aggregate binding. SC-specific knockdown of a negative regulator of Rab11a-exosome biogenesis, the accessory ESCRT-III protein, Chmp5 suppressed the abnormal transfer of GFP-MFAS and endolysosomal propagation phenotype observed when non-cleavable APPL mutants are expressed in SCs, without affecting other GFP-MFAS secretion from SCs. Consequently, my data suggest that Rab11-exosomes may be critical in propagating pathological defects relevant to AD, and that blocking or disrupting of their interactions with protein aggregates may ultimately provide a new therapeutic strategy for treating AD.

Table of Contents

1. Introduction

1.1 Amyloids

1.1.1 A History of amyloid discoveries

In 1854, the German biophysicist Robert Virchow popularised the term amyloid to designate macroscopic tissue abnormalities visible in the cerebral corpora amylacea that exhibited positive reactions to iodine and sulfuric acid staining. Originally, “amyloid” was first proposed to contain a polysaccharide-based structure, from which it derived its name; *amylum* and *amylon* from the Latin and Greek translations of starch, respectively. Later investigations, utilising polarising light-microscopy studies and in-situ Congophilic staining of amyloid deposits, reclassified amyloid as a protein-based molecular structure based on its inherent birefringence pattern [1, 2]. In 1935, the characteristic cross-β-sheet structure of amyloids was identified based on X-ray fibre diffraction films of heat-denatured egg albumin (**Figure 1A**) [3]. Further work by Pauling and Corey theorised that enantiomeric β-sheet peptides co-assemble into so-called “pleated” or “rippled” β-sheet motifs, both of which have been recently confirmed by protein crystallisation (**Figure 1B**) [4, 5]. In current research, the term amyloid has come to encompass a heterogeneous group of self-assembling protein- or peptide-rich aggregates [6] that form micron-length filaments ordered into a densely packed cross β-sheet structure, stacked perpendicularly to the fibril growth axis.

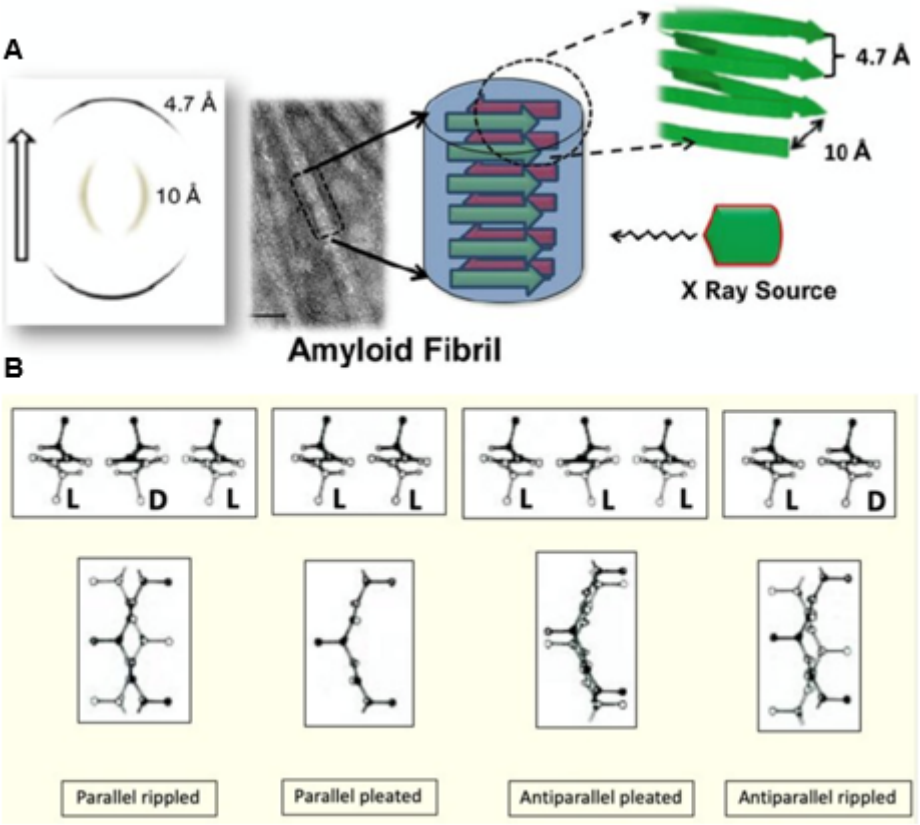

Figure 1: X-ray diffraction and structures of Amyloids.

A. A schematic cross-β X-ray diffraction pattern characteristic of amyloid fibrils. The pattern is consistent with a core of β sheets arranged perpendicular to the longitudinal axis of the fibril. The reflections at 4.7 and 10 Å, represent the inter-strand and the inter-sheet spacing of the cross-beta structure. The white arrow indicates orientation. Figure adapted from [2].
B. The possible structures and orientations of β-sheets, first introduced by Pauling and Corey. In 1951, they predicted pleated-sheet conformations and in 1953, the rippled sheet structure was theorised. Figure adapted from [7].

1.1.2 Amyloids in nature

Amyloid	Amyloid Function	Group	Reference
Peptide hormones	Regulates mammalian sorting, storage, and release of hormones	Group I – Chemical Storage	[8]
Pmel17	Assembles at the surface of melanosomes and provides a scaffolding-template to sequester highly reactive melanin intermediates	Group II - Structural	[9]

Swi1p	A member of the chromatin remodelling SWI/SNF complex that affects transcription and elongation in *S. cerevisiae*, prion form inactive	Group III – Information (also group (IV, loss-of-function)	[10]
Adaptor protein Imd	Imd regulates the immune response in *Drosophila* by interacting with PGRP-LC and PGRP-LE, which subsequently activates the NF-κB pathway	Group V – Gain of Function	[11]

Table 1: Functional Amyloids.

A list of functional amyloids with their corresponding classifications.

Pmel17: premelanosome protein, PGRP: peptidoglycan recognition protein.

In nature, cross β-sheet conformations are amongst the most stable structures, contributing to several classes of 'functional amyloids' with wide-ranging physiological functions: including hormone storage, defence mechanisms, and transcriptional regulation (**Table 1**).

Amyloids present within the seminal coagulum have been implicated in promoting the overall success of reproduction by facilitating the clearing of the female reproductive tract (FRT). In humans, seminal amyloids attach to sperm, immobilizing them and promoting their phagocytosis by immune cells, facilitates appropriate conditions for remating by rapidly clearing the FRT and returning it to its pre-mating state within 24 hours. Furthermore, this process has also been implicated in preventing inappropriate cell-mediated responses against healthy sperm antigens [12]. Whilst relatively few physiological amyloids have been confirmed in humans, their biological functions have been more extensively characterised in *Drosophila* species [13].

1.2 Alzheimer's disease

1.2.1 Dementia

Errors in the process of protein processing and multiprotein assembly can result in amyloidosis, or the accumulation of misfolded amyloid-like oligomers which can lead to cell death. Their intrinsic misfolded nature and aggressive proclivity to aggregate grant them unique structural, kinetic, and cytotoxic properties [14], distinct from their functional counterparts. Such properties mediate their involvement in abnormal interactions with a wide range of cellular targets.

Dementia is an umbrella term comprising a heterogeneous group of neurodegenerative diseases characterised by a significant decline in cognition. Alzheimer's Disease (AD) is the most prevalent form of dementia, accounting for 60–80% of total cases and remaining the most extensively researched amyloidogenic disease [15]. AD manifests as a progressive decline in episodic memory and cognitive functions, resulting in deficiencies in language and visuospatial skills, which are often accompanied by neuropsychiatric symptoms such as depression, aggression, and psychosis. The prevalence of AD increases significantly in individuals over the age of 50, affecting approximately 22% of the global elderly population above the age of 50 through all of its classification stages (**Figure 2**).

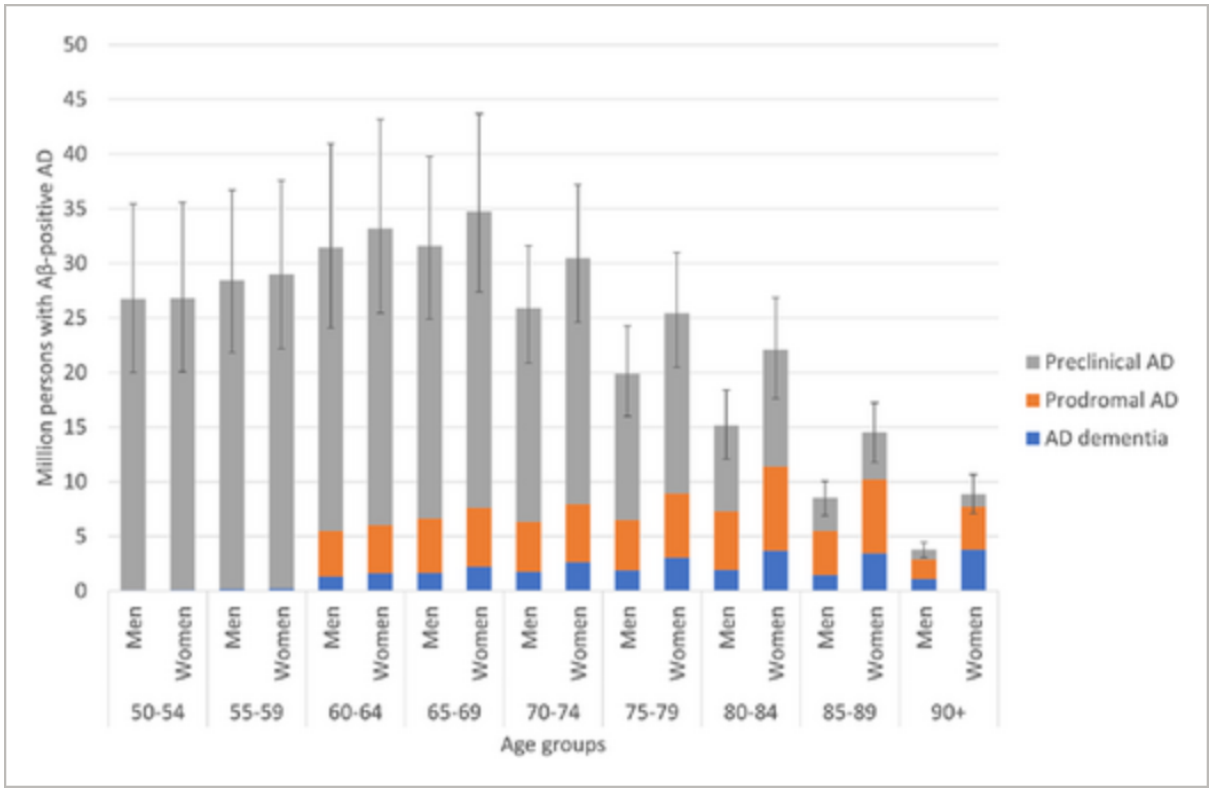

Figure 2: Schematic displaying the epidemiology of AD.

Estimated number of individuals with AD, estimated by age, sex, and classification stage. Derived from worldwide data (https://population.un.org/wpp/), which reveals an estimated global disease burden of 416 million individuals [16, 17].

1.2.2 Mutations that cause AD

AD is classified as Familial (fAD) or sporadic AD (sAD). sAD presents as an idiopathic condition, driven by the complex interplay of genetic and environmental factors. In contrast, familial AD (fAD), which accounts for between 5-10% of diagnoses, is usually driven by single nucleotide polymorphisms (SNPs), primarily localised around the *Amyloid Precursor Protein* (*APP*), *presenilin-1* (*PSEN1*), and *presenilin-2* (*PSEN2*) genes. Despite the difference in their underlying causes, both fAD and sAD often lead to similar pathological outcomes.

1.3 The molecular mechanisms underlying AD

1.3.1 AD can be mediated by Amyloid-β (Aβ)

The AD-brain is characterised microscopically by the presence of two hallmark proteinaceous aggregates: extracellular neuronally synthesised amyloid (Aβ) plaques and intraneuronal Tau-containing neurofibrillary tangles (NFTs) **(Figure 3**) [18]. The amyloid cascade hypothesis proposes that the deposition of Aβ-peptides in plaques in the brain is the "*causative agent of Alzheimer's pathology,"* responsible driving the pathogenesis of Tau and other aggregating proteins [19]. This Aβ-peptide accumulation results in the disruption of physiological cellular processes including proteostasis, mitochondrial function, and genomic stability [20].

In humans, Aβ deposition follows a distinct "top-down" anatomical progression, initially described by Thal and colleagues [21], in which amyloid deposits accumulate in regions with elevated neuronal activity and spread through synaptically connected regions or are endocytosed into other cells [22].

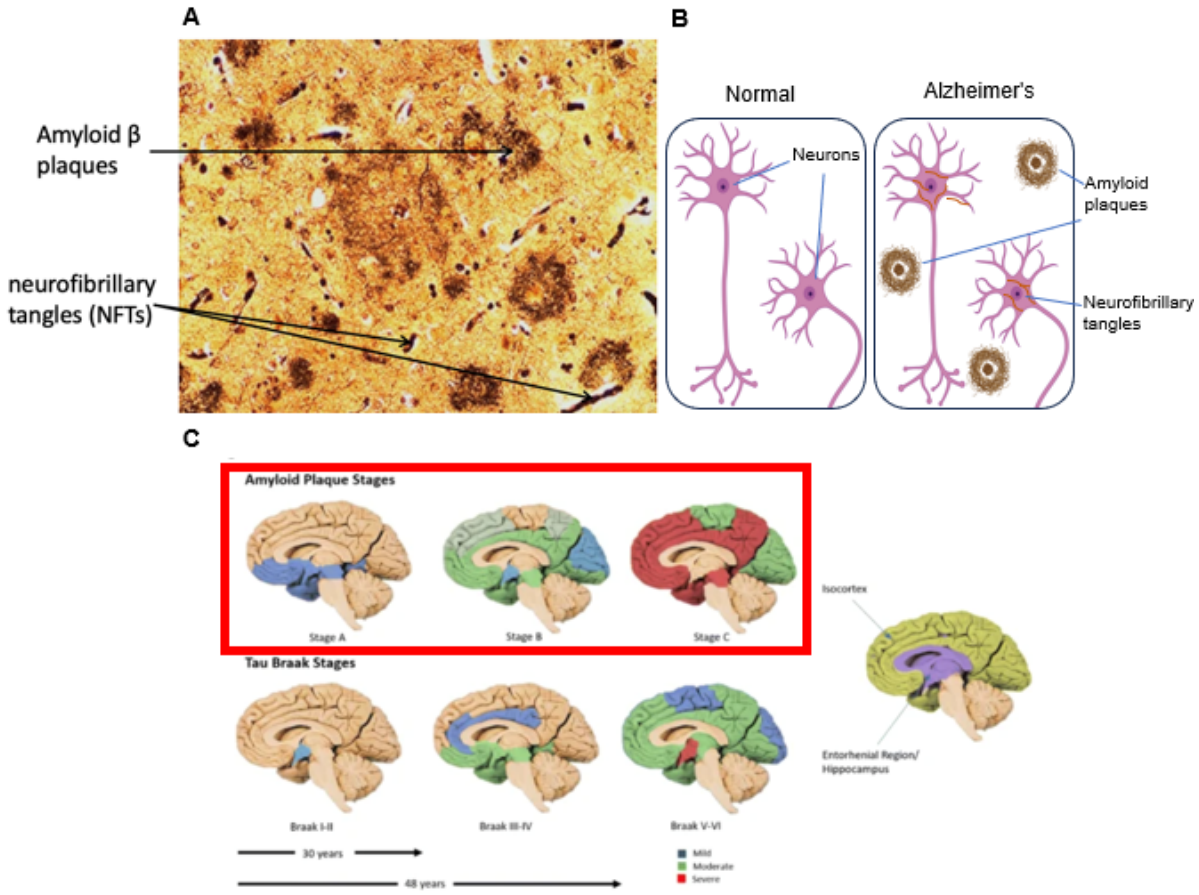

Figure 3: Hallmark Proteins of Aggregations of AD and their spread.

A. Picture of a brain slice of an AD brain, with abnormal proteins labelled.
B. Illustrations of tissues taken from a normal and AD brain.
C. Integrating the Thal (Aβ) and Braak and Braak (Tau) schemes of deposition (from ref. [21]). Amyloid β progression [Boxed in Red] is split into three stages, firstly accumulating in the entorhinal cortex (Stage A). In stage B, β-amyloid propagates into the hippocampus and associated neocortices. It finally extends into the cerebellum, subcortical nuclei, and primary cortices (Stage C). Amyloid plaques have been recorded in patients, as early as 48 years before clinical diagnosis. The onset of clinical AD is preceded by a long asymptomatic phase, comprised of a complex series of molecular and cellular events, referred to as the amyloid cascade hypothesis [23].

1.3.2 APP and its proteolysis via the amyloidogenic pathway

Aβ-peptides are generated through sequential endoproteolytic cleavages of amyloid precursor proteins (APP), a type I transmembrane protein. APP is expressed in both neuronal and extra-neuronal tissues. While its roles are not yet fully understood, several functions have been identified. These include it's role mediating neuronal growth, synaptic plasticity, and

maturation during brain development; potentially by influencing the cell fate specification and neurogenesis of neural stem cells (NSCs) [24, 25]. APP undergoes sequential proteolytic cleavages by integral membrane α-, β-, and γ-secretases, following either the non-amyloidogenic or amyloidogenic pathways (**Figure 4**). In addition, APP can be cleaved in other, less well-described pathways, including meprin-β cleavage, the *δ*-pathway and the *η*-pathways [26].

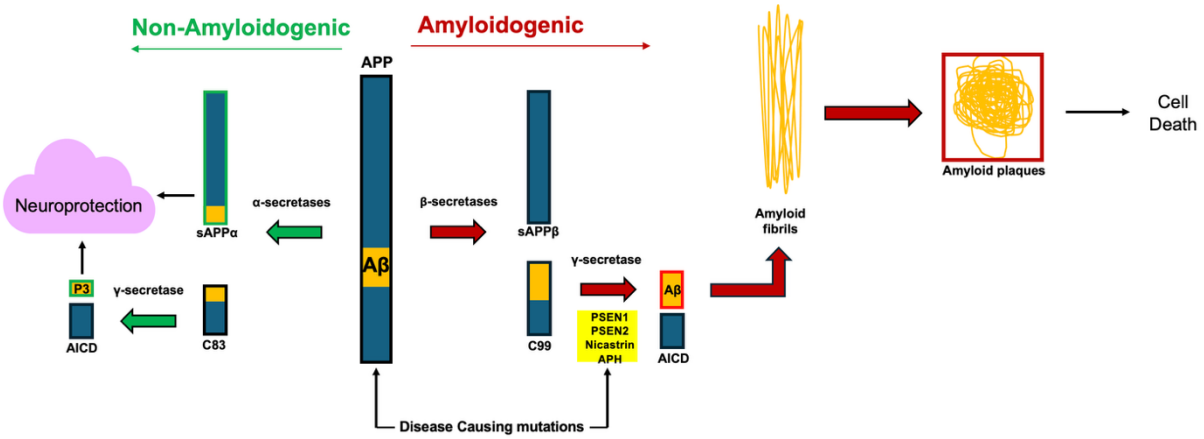

Figure 4: Pathways of APP Processing.

In the non-amyloidogenic pathway, the initial cleavage of APP is processed by α-secretase [37], producing a truncated extracellular (or luminal inside endosomal compartments) fragment (sAPPα) and C83, which can be further cleaved by via γ-secretase, generating a soluble extracellular Aβ p3 peptide with neuroprotective properties. In the amyloidogenic pathway, APP is cleaved by β-secretase (BACE, β-site APP-cleaving enzyme 1), releasing sAPPβ and C99. C99 is subsequently cleaved by the γ-secretase enzymatic complex, highlighted in yellow (PSEN1, Presenilin 1; Nicastrin; Aph-1, anterior pharynx-defective 1 and Pen-2, presenilin enhancer 2), releasing a cytoplasmic polypeptide, AICD (APP intracellular domain) and extracellular Aβ peptides. Aβ can be secreted into the extracellular space from endosomes.

1.3.3 Amyloid beta (Aβ)

The pathological cleavage of the 99 amino acid membrane-bound C-terminal fragment (C99) by γ-secretase takes place at several sites, producing Aβ-peptides with various C-terminal ends. In AD, disease-associated mutations favour the formation of aggregation-prone $A\beta_{42\text{-}43}$ species at the expense of shorter, $A\beta_{40}$ peptides [27]. NMR-guided simulations have demonstrated that these longer-chained Aβ-sequences undergo structural alterations that

enhance their propensity to form amyloid fibrils [28, 29]. Although Aβ generation can occur at the plasma membrane where it is released extracellularly, the majority of amyloidogenic-Aβ is generated intracellularly in endosomes and secretory compartments.

1.3.4 Intra-Aβ mutations

FAD mutations are distributed across the entire length of *APP* molecule*;* however, many cluster within or at sites adjacent to the canonical $A\beta_{42}$ region (**Figure 5**). These "classical" fAD mutants are localised around the α-, β-, and γ-secretases sites, and mass spectrometry analysis has revealed that this proximity underlies their abilities to influence proteolytic processing [30]. As a result, generating distinct Aβ peptide profiles, which are associated with an enhanced vascular amyloid deposition which commonly leads in haemorrhagic stroke and early fatality in patients [30, 31].

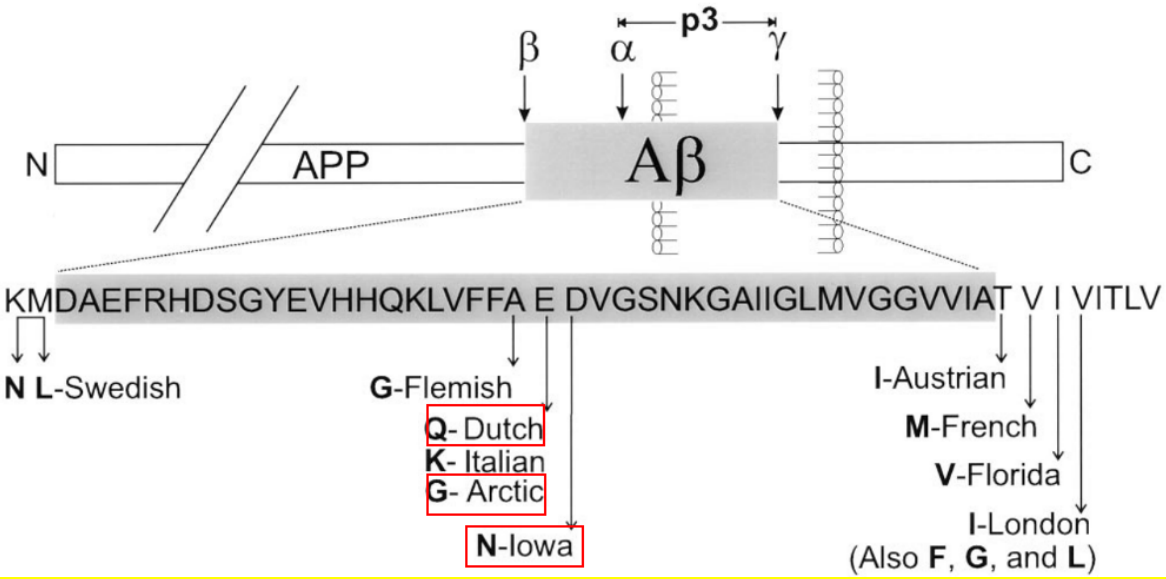

Figure 5: APP molecule with $A\beta_{42}$ region highlighted.
Human APP_{695} molecule, with N and C terminal domains illustrated alongside $A\beta_{42}$ sequence, with α-, β-, and γ-secretases sites and known fAD mutations that cluster around these sites listed with their amino acid substitutions. Mutations around the α-secretase, Q-Dutch, G-Arctic, and N-Iowa are boxed in red and are analysed in this study. Figure adapted from [32].

In this study, I focused three APP variants carrying mutations surrounding the α-, secretase cleavage site within the $A\beta_{42}$ sequence, E693G (Arctic mutation), E693Q (Dutch mutation),

and D694N (Iowa mutation). Evidence has shown that both Arctic and Iowa mutants perturb APP trafficking and processing in a manner that promotes the early stages of the pro-amyloidogenic pathway [30, 33].

Interestingly, the mechanisms by which these alterations occur underlie the pathological hallmarks characteristic in patients with fAD mutations. In the Arctic variant, the presence membrane-bound Arctic-APP at the cellular surface is diminished and internalised into endosomal compartments, where they are preferentially cleaved by β-secretases [33]. In transgenic mice aged six months, Arctic mutations form stable intraneuronal Aβ deposits that present concomitantly with cognitive impairment and behavioural deficits. Over time, these intracellular Aβ deposits, oligomerise into Aβ-plaques with a characteristic “dense core” morphology alongside cerebral amyloid angiopathy (CAA), which differ from cotton wool-like structure of plaques seen with in other fAD mutants (**Figure 6**) [34].

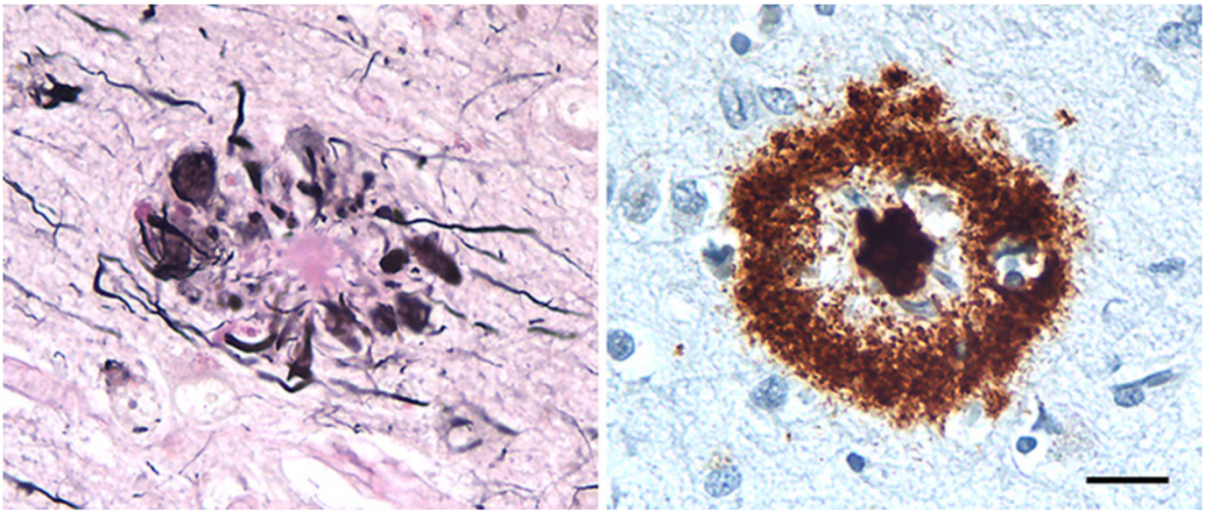

Figure 6: A human cortex slice of persons who have died with fAD Alzheimers Disease.

Left, characteristic Aβ ‘cotton wool’ plaque pathology, visualised with Naoumenko-Feigin silver staining and periodic acid-Schiff (PAS) counterstain. Right, a “dense core” in a patient carrying the Arctic mutation, immunostained with antibody 4G8 to the Aβ protein (brown) along with a Nissl counterstain (blue); Scale 20μm.

1.3.5 Endosomal pathway dysfunction as an early biomarker of Alzheimer’s Disease

The endosomal pathway is tasked with internalising, modifying, and packaging extracellular nutrient and trophic factors for release. It does this by guiding cargoes through a series of conserved pathways that coordinate either their recycling, degradation, or secretion. In neurons, endosomal dysfunction is a seminal pathology in AD, being its earliest known cytopathology, often presenting decades before traditional amyloid pathology [35].

Early endosomes (EEs) act as the first major sorting station of the endosomal pathway, providing a “pathologically acidic” environment that complements the processing of AD-associated proteins, including APP by β-secretases and facilitates its complexing with AD-risk genes such as apolipoprotein E (ApoE) and Bin1 [36]. In pre-AD human brain slices, neuronal EEs confined to the neocortex were found to be several-fold larger than normal, reflecting morphological changes consistent with the aberrant upregulation of endosomal activity, characteristic of AD pathology [35].

Endosomal trafficking is regulated by members of the Rab GTPase family, which act as molecular switches to modulate endosomal dynamics by recruiting specific effector proteins [37]. Rab5 localises to the membranes of early endosomes, where it coordinates endosomal fusion and docking events to regulate cargo trafficking and direct downstream trafficking. In AD patients, Rab5 is commonly upregulated/hyperactivated, and it lines the surface of these enlarged Rab5 positive-EEs. In these compartments, an increase in levels of β-cleaved APP C-terminal fragments are frequently detected - an essential precursor in Aβ generation [38].

A paired RNAi and RabGAP overexpression screen all human Rab-GTPases, which regulate membrane trafficking has identified Rab11, as an important regulator of β-secretase-mediated APP processing [39]. Their aberrant overexpression on the surface of mature endosomes resulted in an increased production of sAPPβ and Aβ [39]. Rab11 primarily mediates a slow recycling pathway (delivering cargo protein form the early endosomes back to the cell surface), which has been proposed to play a central role in AD pathogenesis.

In this “hub-and-spoke” model, the recycling pathway acts a pathogenic hub from which AD-related pathologies including amyloid, tau, and microglia disseminate in parallel, as opposed to a linear cascade [40]. This proposed model resolves several key inconsistencies within traditional amyloid hypothesis by integrating it with the endosomal pathway. Whilst it has been established that this pathway regulates post-translational processing and targeting of APP, modulating its associations with secretases and risk-proteins, its broader role in AD is still being uncovered.

Genome-wide association studies (GWAS) have identified novel endocytic risk loci such as SORL1 and RIN3 that interact directly with the APP molecule and its cleavage products [41, 42]. These developments highlight the critical need for improved in vivo models to investigate these secretory pathways and determine the functional consequences of these proteins in disease contexts.

1.4 Using *Drosophila* to model AD.

1.4.1 APPL is the *Drosophila* orthologue of human APP

Mammals express three closely related members of the APP family: APP, Amyloid precursor like protein 1 (APLP1) and Amyloid precursor like protein 2 (APLP2) (**Figure 7A**). Despite extensive research efforts, traditional models have often failed to isolate the discrete molecular functions of individual APP family members, seemingly because of redundancies in model systems [43]. In mice, the phenotypes produced by single APP knockout studies are often minimally penetrant, with double and triple APP family knockouts exhibiting perinatal lethality [43]. Thus, *Drosophila* has emerged as an attractive alternative for the analysis of AD due to its well-curated genome and diverse genetic toolbox.

.

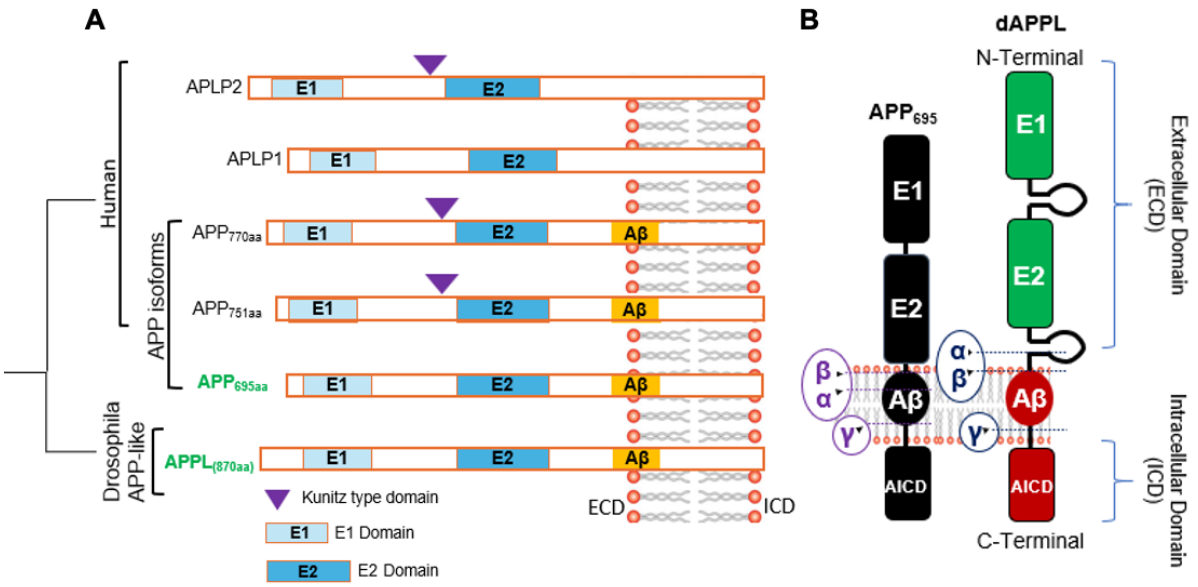

Figure 7: Schematic of APP family members and its *Drosophila* Isoform.

A. Displayed are 5 isoforms of APP and Amyloid Precursor-Like Proteins APLP present in humans, which range from 659 to 870 amino acids in length displayed alongside the *Drosophila* orthologue of APP, APPL. APPL shares the highest degree of identity with APP_{695}, (both shown in green), which is most abundantly expressed in neurons.
B. Displayed is a schematic comparing APPL and Human APP_{695} structural organisation, with their highly conserved regions including their ectodomains (E1 and E2 regions) highlighted in green and intracellular domain in red.

The fly genome contains a single APP family member, APP (App-like), which facilitates loss-of-function studies. Despite a limited conservation between specific protein primary sequences, APPL contains analogous reversed α-, β- and γ-secretase cleavage sites (**Figure 7B**) capable of generating extracellular cleavage products – such as Aβ-like peptides, which can form amyloid deposits and elicit age-dependent behavioural deficits and neurological degeneration, mirroring aspects of human pathology [44].

Notably, *Appl* loss-of-function phenotypes can be partially rescued by human APP, highlighting the gene's functional conservation [45]. In *Drosophila*, initial research efforts to characterise the molecular and subcellular functions of APPL have yielded positive results. In a paper by Dr. Nithianandam and colleagues at Harvard University, APPL has been implicated in

modulating a wide range of physiological processes, including translation, mitochondrial function, cellular signalling, and proteostasis during ageing [46].

This novel research focus on APP's subcellular functions comes in response to significant limitations in the amyloid hypothesis, as many healthy older adults show significant amyloid deposition without displaying cognitive symptoms [47]. This suggests Aβ may initiate neurodegeneration via intracellular mechanisms involving APP that are yet to be defined (see Section 1.3.5).

1.4.2. The genetic toolbox of *Drosophila*

Drosophila melanogaster possesses a well-curated genome, with approximately 75% of genes that are associated with or that cause human diseases having orthologues in the fly genome, and the vast majority of fundamental cellular and molecular processes conserved between fly and humans [48, 49]. This evolutionary conservation, combined with open-access genetic tools and resources from databases like FlyBase, and the Bloomington *Drosophila* Stock Center (BDSC) establishes *Drosophila* as an accessible and powerful system for modelling human disease mechanisms.

I employed the yeast GAL4-UAS system for spatiotemporal control of transgene expression – combined with a ubiquitously expressed temperature-sensitive repressor (tubulin-GAL80ts) [50]. Balancer chromosomes enable stable maintenance of mutations in fly stocks. Coupled with *Drosophila's* rapid generation time, this approach allows for high-throughput generation of experimental populations with precise genetic parameters.

1.5 Using a novel prostate model to investigate secretory functions

1.5.1 An overview of the accessory gland (AG) and its cell types

Previous work by the Wilson Group has pioneered the use of the male accessory glands in *Drosophila* to model different aspects of secretory dysfunction associated with early-stage AD (**Figure 8)** [51]. In addition to the testis and seminal vesicles, the male reproductive system in *Drosophila* comprises paired accessory glands (AGs), an ejaculatory duct, and ejaculatory bulb. The AGs are the main producers of seminal fluid constituents, analogous to the prostate and seminal vesicle systems present in mammals [52].

Each AG lobe is lined with a monolayer epithelium surrounded by a muscular sheath, which contracts during mating to excrete about one-third of the gland's contents. This epithelium consists of two types of secretory cell types, exhibiting distinct patterns of gene expression [53]: around 1000 main cells (MCs) interspersed with 40 secondary cells (SCs) localized at the apical tip of each accessory gland lobe [54] (**Figure 8**).

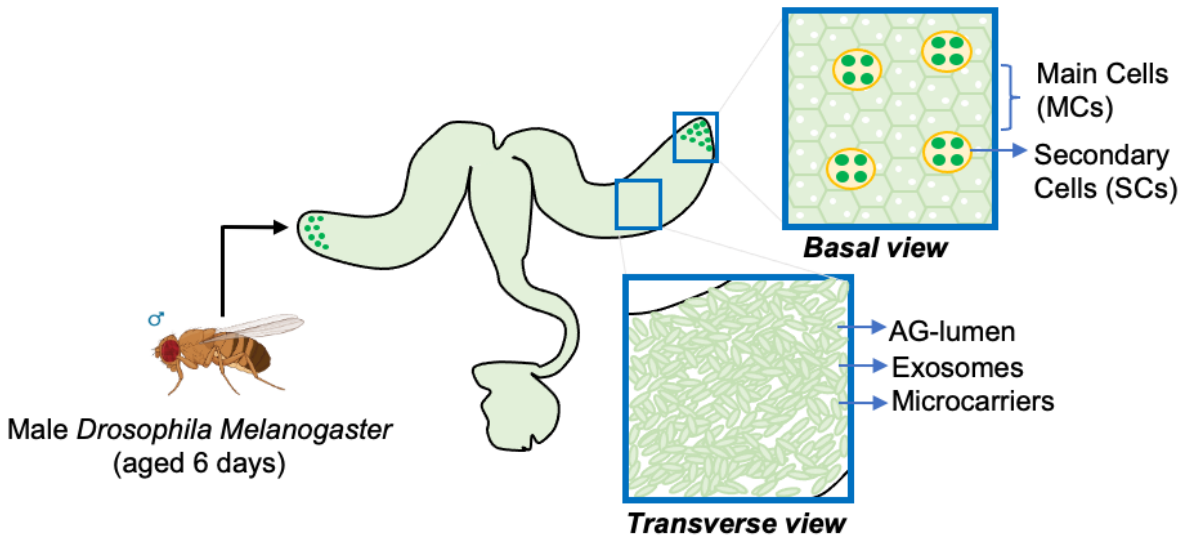

Figure 8: The male reproductive system of *Drosophila.*

A schematic showing the male accessory glands, lined with a monolayer epithelium formed from two secretory cell types: binucleated main cells (MCs) and secondary cells (SCs). The latter is located at the apical tip of each accessory gland lobe [54]. Note that each mature large secretory compartment in SCs contains a DCG, marked by GFP-MFAS (green; expressed from the endogenous *mfas* locus), the *Drosophila* orthologue of amyloidogenic protein TGFBI. *Drosophila* APP-like (APPL) controls DCG aggregation through membrane-associated priming and subsequent aggregate release following APPL cleavage.

1.5.2 Secretory cells of the AG and their involvement in female post-mating responses

Sexual reproduction requires the choreographed interaction of female cells with sperm and seminal fluid. MC secretions mediate post-mating responses (PMRs) in inseminated females via Sex Peptide (SP), and other seminal fluid proteins [SFPs] [55]. Targeted cell ablation of MCs or *SP* loss-of-function in males blocks female long-term post-mating responses, including egg-laying and receptivity to remating [56, 57].

In recent studies, SCs have also been implicated in modifying the female PMR, with their abnormal development in iab-6(cocu) males being associated with a reduction in female egg laying and female receptivity over time [58]. This has been attributed to specific genes and proteins within SCs that have been implicated in sustaining the PMR past 24 hrs by allowing SP to bind to and be stored with sperm.

The secretion of SC-proteins is mediated by an autocrine BMP feedback loop mechanism and some paracrine signalling between SCs [59, 60]. Upon mating, secretory compartments are released from SCs. These compartments contain specific signalling molecules, including Decapentaplegic (DPP), the *Drosophila* homologue of the mammalian Bone Morphogenetic Protein (BMP) ligands BMP2 and BMP4 (**Figure 9**). This BMP ligand accelerates the formation of new secretory compartments in preparation for subsequent matings. Blocking this pathway in adult males selectively blocks the post-mating effect of males on female receptivity [59].

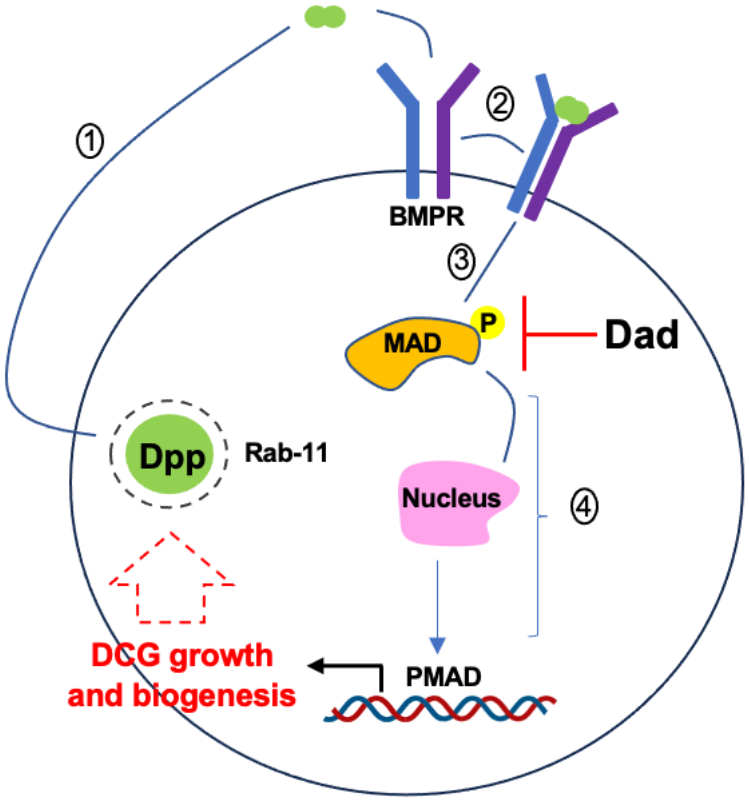

Figure 9: Autocrine BMP-feedback loop.

Schematic representation of the signalling regulation of DCG growth: (1) DCGs exhibit a basal level of Dpp secretion from Rab11-positive DCG compartments. (2) Dpp dimerizes BMP type I and II receptors, (3) resulting in the phosphorylation of the protein mothers against dpp (MAD), a process negatively regulated by DAD. (4) pMAD translocates into the nucleus, activating transcription factors that promote rapid DCG compartment biogenesis and cell growth. Figure adapted from [59].

1.5.3. Secondary cells as a model for regulated secretory biology

The Wilson Group has developed SCs as a model to study regulated secretory biology, as they exhibit a high degree of conservation with secretory cells in mammalian glands. *Drosophila* SCs selectively package signalling molecules into massive DCG compartments, thousands of times larger than their human neuronal equivalents, allowing dynamic intra-compartmental maturation events to be visualised by fluorescence microscopy [51, 61].

DCG compartments contain intraluminal vesicles (ILVs), that are released as exosomes upon compartment fusion with the plasma membrane. DCG compartments are lined with

intraluminal vesicles (ILVs) [61]. Since these ILVs are not generated in late endosomes, but in compartments labelled with recycling endosomal marker Rab11, these Rab11-exosomes are packaged with distinct cargos [62, 63].

Physiologically, DCG compartments act as specialised secretory organelles that are abundantly expressed in neurons and the neuroendocrine system, where they facilitates the packaging and regulated release of complex neuropeptide and hormone molecules [64]. Their formation involves a series of membrane trafficking and maturation events mediated by a dynamic interplay of GTPases of the Rab family, sorting complexes and adaptor and aggregating proteins (**Figure 10**) [63]. In these compartments, a Rab6 (trans-Golgi-associated) to Rab11 (recycling endosome-associated) transition is essential for DCG and Rab11-exosome biogenesis [61], a process that is highly conserved between *Drosophila* and humans [61, 65].

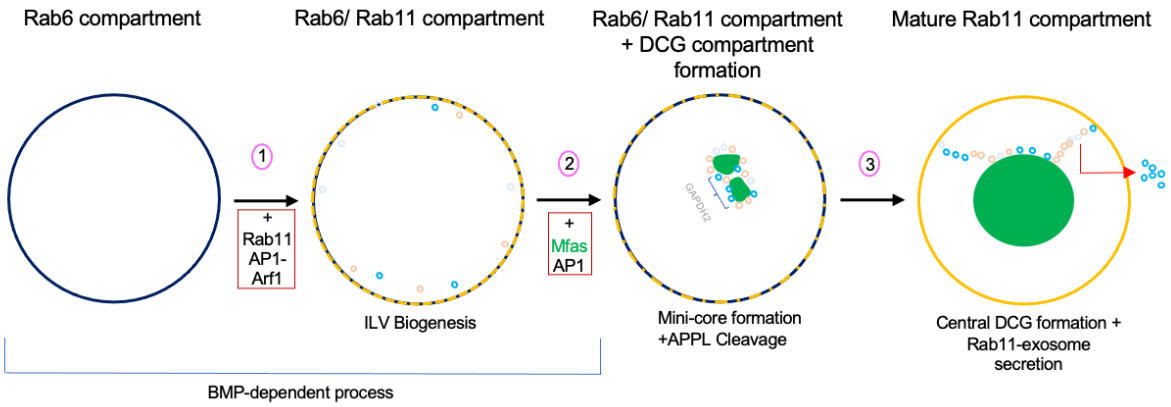

Figure: 10: A Rab6 to Rab11 model of DCG biogenesis and function in the SCs *Drosophila* model.

A schematic outlining the maturation and formation of DCG compartments: (1) A core-less Rab6-positive compartment recruits Rab11, a process regulated by a ADP-ribosylation factor 1 (Arf-1) and adaptor protein complex 1 (AP-1) complex - inducing the formation of ILVs (blue, gold and grey circles), a process dependent on accessory ESCRT-III proteins, such as CHMP5. (2) MFAS (green) appears to be delivered to the compartment at this stage; APPL triggers mini-core fusion, a process dependent on ILVs, and their clustering by GAPDH. These stages are regulated by BMP-dependent signalling. 3. APPL cleavage triggers mini-core release from ILVs and the compartment limiting membrane, and these structures fuse to form a large central DCG with clusters of ILVs lining its periphery and attached to the compartment's limiting membrane. Extravesicular GAPDH2 is required for this clustering. These are secreted as Rab11-exosomes (blue circles). This figure is adapted from [61].

1.5.5 APP regulates DCG maturation, which is disrupted by blocking APP cleavage or expressing Aβ

Previous research by members of the Wilson Group investigating the physiological roles of transmembrane APPL has identified that it traffics into immature Rab6-labelled DCG precursor compartments, where it lines compartment membranes and is involved in DCG aggregate priming. It is then proteolytically cleaved, permitting MFAS-containing DCG proteins to coalesce into a central DCG core.

Expressing APPL or Aβ-mutants in SCs has revealed that failure to cleave APP or overexpression of amyloidogenic Aβ-mutants "aborts" this maturation process, resulting in DCGs exhibiting membrane-associated 'misshapen' and mini-core phenotypes that are aberrantly targeted to lysosomes [51] (**Figure 11**). The resulting GFP-MFAS protein is still secreted and is more readily endocytosed into neighbouring normal main cells (MCs), generating larger abnormal lysosomal compartments in those cells localised at the apical tip of AGs [51]. Impaired lysosomal function, disruption in secretory processes, and propagation of pathology have all been implicated as fundamental and potentially initiating defects in AD pathogenesis.

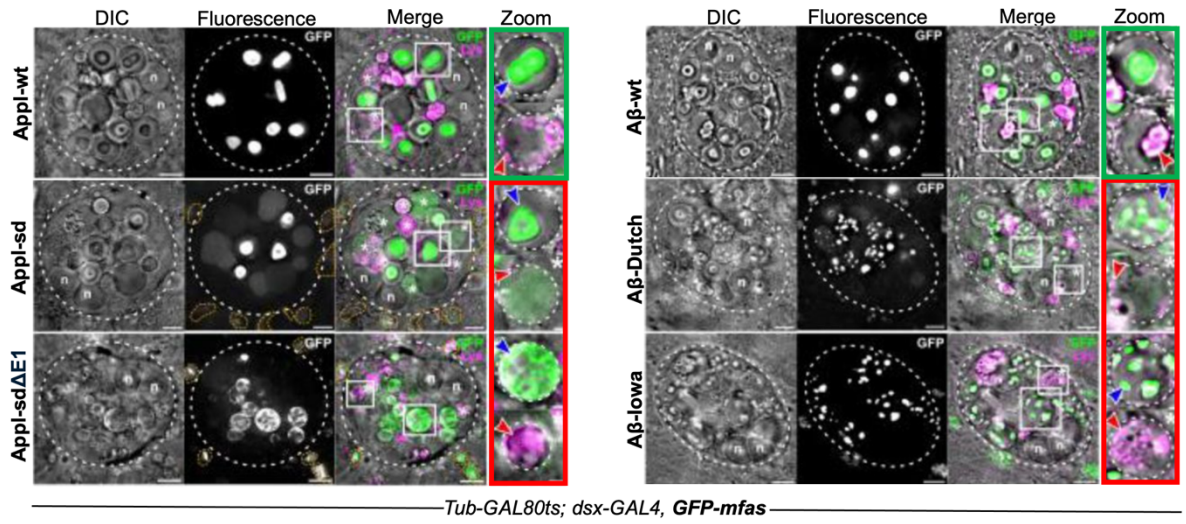

Figure 11: Expressing Appl mutants and pathological Aβ-42 peptides in SCs disrupts DCG biogenesis.

Ex vivo, wide-field fluorescence micrographs and DIC images were captured of SCs expressing a *GFP-mfas* gene trap and either mutant Appl proteins or Aβ-mutants. Displayed on the left are SCs expressing a *GFP-mfas* gene trap and wild-type APPL (APPL-WT) controls, APPL-Δsd or APPL-ΔsdE1. On the right-hand side are SCs expressing the same gene trap, but co-expressing $A\beta_{42}$ mutants Iowa or Dutch or wild type Aβ-42. Note, DCG compartments in merge panels surrounded with a white box display an abnormal DCG phenotype (upper zoom; panel blue arrowhead) and acidification phenotype (lower zoon panel; red arrowhead) much more frequently when mutant APPL or Aβ is expressed (from reference [38]). Also, expression of these mutated molecules leads to GFP-MFAS accumulation in neighbouring MCs, lying outside the SC boundary, which is marked with a dashed white line; these are most clearly seen in the GFP-only channel. (Figure adapted from [51]).

1.6. Summary

To date, the lysosomal phenotypic propagation generated by mutant non-cleavable forms of APPL and mutant-Aβ have only be studied in the apical tip of the AG. In this project, I extended this work, examining whether such phenotypes propagate across the entire AG epithelium. By exploiting the AG's luminal secretion model, I was able to investigate the mechanisms underlying the release of SC-derived cargoes, how these influence their endocytic uptake by neighbouring MCs, and the release of internalised materials via mating (induced partial lysosomal turnover) and subsequent recovery.

Through this approach, I aim to present an argument for the use of Drosophila as a high throughput model to AD, and its pathology. Specifically, I hope to show that the discreet and variable phenotypes induced by individual AD-mutants (absent of any cell autonomous endolysosomal defects) can be accurately recapitulated by the SC-secretory mechanisms within the prostate gland, which resemble the packaging processes within the neuronal system within human AD. In addition, I show that this "propagation phenotype" is dependent on a distinct subtype of exosomes, produced as a product of the endosomal recycling pathway and independently of the other SC secretions.

Together, these findings highlight the AG model as a versatile platform to probe the molecular mechanisms underlying APP/Aβ biology and secretory trafficking. In doing so it has the potential to refine the current understanding of the early events in AD pathogenesis and

provide new insights into how pathological phenotypes emerge and propagate across tissue types.

1.6.1 Project aims

The key aims of my project were to:

- Quantify the propagation of GFP-tagged MFAS protein from SCs to MCs throughout the accessory gland epithelium following SC-specific expression different Aβ and non-cleavable APPL mutants.
- Assess the fate of endocytosed GFP-MFAS and MC lysosomal compartments following mating and a recovery period after mating.
- Determine the role of SC secretion and exosome biogenesis in endocytic uptake of GFP-MFAS by MCs.

2. Materials and Method

2.1 Fly stocks and husbandry

All *Drosophila* strains used in this project are listed in **Resource Table 2** below. The transgenic lines were sourced from the Bloomington *Drosophila* Stock Centre (BDSC), donated by other laboratories, or generated through microinjection by the Faculty of Genetics at the University of Cambridge. Other recombinant stocks were generated by members of the Wilson Lab, unless otherwise stated. To create temperature-dependent, inducible driver lines, *dsx-GAL4* was combined with *tub-GAL80^{ts}*, a ubiquitously expressed GAL4 repressor, forming *tub-GAL80^{ts}; dsx-GAL4*. This driver line was further recombined with a GFP-tagged *mfas* gene trap to visualise DCG biogenesis and transfer of aggregating material between cell types.

Flies were reared at 25°C with 60% humidity on a 12-hour light/dark cycle using a standardized BDSC cornmeal medium. This medium consists of 12.5 g agar, 75 g cornmeal, 93 g glucose, 31.5 g inactivated yeast, 0.7 g calcium chloride dihydrate, and 2.5 g nipagin dissolved in 12 ml ethanol per litre. Flies were maintained in 10 cm³ polystyrene vials (Regina) plugged with non-absorbent cotton balls (Fisherbrand®) or in larger semi-transparent plastic bottles (Fisherbrand®) sealed with disposable synthetic foam plugs. They were transferred to fresh media every 5-6 days. Virgin female flies carrying *tub-GAL80^{ts}; dsx-GAL4, GFP-mfas*, were crossed with male flies carrying UAS-transgenes to induce a SC AD-related overexpression phenotype. These crosses were maintained at 25°C. Upon eclosion, virgin male offspring were collected and kept at 29°C for six days to inactivate GAL80 and promote post-developmental, SC-specific transgene expression in the accessory gland. The aged offspring were either dissected as virgins or mated with single *w^{1118}* females aged to the same developmental stage. After mating, the flies were separated to prevent re-mating and the female reproductive tract (FRT) and male AG were dissected out at zero, three-hours post-mating.

Table 2: A list of drosophila stocks used for this investigation.

Stocks	Description	Source

DTMFAS *w; tub-GAL80ts/CyO; dsx-GAL4 GFP-mfas/TM6*	Expresses GFP-MFAS from gene trap and dsx-Gal4, the accessory gland SC-specific driver with Gal80 under the control of an α-tubulin temperature specific promoter	Lab made stock
w^{1118}	Non-transgenic control line for GAL4 crosses	Partridge Lab, UCL
Appl-wt *w^{1118}; UAS-Appl.T*	Allows expression of wild type Appl under GAL4/UAS control	BDSC - 38403
Appl-Δsd *w^{1118}; UAS-Appl-sd*	UAS sequences control expression of a form of Appl with α- and β-secretase cleavage sites deleted	BDSC - 29865.
Appl-sdΔE1 *w^{1118}; UAS-Appl.sd DeltaE1*	UAS sequences control expression of an Appl-sd protein lacking amino acids 85-321, which includes part of the E1 domain	BDSC - 29866
$Aβ_{42}$ Dutch *w^{1118}; UAS-$Aβ_{42}$E693QDutch*	Expresses a fusion between an ER signal sequence and the human $Aβ_{42}$ fragment of APP carrying the familial Alzheimer's 'Dutch' mutation (APP; E693Q) under the control of UAS sequences	BDSC - 33776
$Aβ_{42}$ Iowa *y; UAS-$Aβ_{42}$D694NIowa*	Expresses a fusion between an ER signal sequence and the human $Aβ_{42}$ fragment of APP carrying the familial Alzheimer's 'Iowa' mutation (APP;D693N) under the control of UAS sequences	BDSC - 33779
$Aβ_{42}$ Arctic	Expresses a fusion between an ER signal sequence and the human $Aβ_{42}$ fragment of APP carrying the familial Alzheimer's 'Arctic' mutation (APP; E693G) under the control of UAS sequences	BDSC - 33774

w^{1118}; UAS-Aβ$_{42}$E693GArctic		
Appl-Δsde1 x DTMFAS *W; UAS-Appl-sdΔe1 tub-GAL80ts/CyO; dsx-GAL4 GFP-mfas/TM6*	Recombinant line, expressing UAS-Appl-sdΔe1	Bhavna Verma – Lab made stock
DAD *w*^{1118}; UAS-DAD	Expresses DAD under the control of UAS regulatory sequences	Daimark Bennett
DPP *y*^{1} *v*^{1}*; P{TRiP.JF02794}attP2*	Expresses dsRNA targeting *dpp* under UAS control	BDSC - 33767
Chmp5 (RNAi - Vps60) *P{KK109120}VIE-260B*	Expresses dsRNA targeting *Chmp5* (*Vps60*), encoding a protein in the accessory ESCRT-III complex, under UAS control	VDRC - 101422
GAPDH2 *y*^{1} *v*^{1}*; P{TRiP.JF02072}* *attP2 - Gapdh2*	Expresses dsRNA targeting *GAPDH2* controlled by UAS sequences	BDSC - 26302

2.2 Imaging and dissection

Accessory glands were dissected and prepared for confocal analysis as described in [62] and [66]. Adult flies were anaesthetised using a diffused stream of CO_2 administered by a Flypad (FlyStuff). The anaesthetised flies were transferred onto a convex microscope slide and placed under a dissection microscope (Meiji Techno - EMZ binocular microscope with MA502 10x eyepieces) illuminated by a swan neck light box (Zeiss LM600).

During the micro-dissection procedure, flies were submerged in ice-cold 1X paraformaldehyde in PBS (PFA). AGs were removed from male flies by carefully extracting the reproductive tract from the abdomen using forceps (Dumont). The testes, seminal vesicles, anterior ejaculatory duct, and ejaculatory bulb systems were removed from AGs to prevent obscuring or compressing of the gland during imaging. In addition, excess tissue and the digestive system were excised and removed.

The tissues were allowed to fix at room temperature for 20 minutes, following which, the AG was repeatedly washed using PBS and mounted onto Frosted microscope slides (Academy, 76 x 26 mm). Excess PBS was removed using Whatman paper, and the tissues were immersed in Vectashield/DAPI mounting media (Vector Laboratories), stably positioned with a coverslip (22 mm x 22 mm, 0.13-0.17 mm) and sealed using a vitamin topcoat nail polish.

As previously described in [66], fixed samples were imaged using a Zeiss LSM980 upright confocal microscope equipped with Airyscan 2. Imaging was performed at 10x magnification (Zeiss 0.45 NA; dry) and 40x magnification (Zeiss 1.4NA; immersion oil, 1.518 refractive index). High-resolution images were acquired using the Zeiss 'Zen Blue' software. The image profile is displayed in **Figure 12,** with DAPI, GFP and DIC settings kept consistent to ensure a uniform fluorescence intensity.

2.3 Image analysis

Images were analysed using Fiji/ImageJ. Five 40x40 pixel boxes were positioned within the flattened epithelial layer of each AG image to measure MC uptake of GFP-MFAS, focusing on regions with an even spread of aggregates, with areas lacking fluorescence and those surrounding folds being avoided (**Figure 12**). To generate a value for luminal intensity, two 90x90 pixel boxes were placed in images captured from the central luminal part of the AG (**Figure 12**). To measure %GFP-MFAS uptake, a flat area of 300x300 pixels was selected,

from which MCs were counted manually, and those with internalised GFP-MFAS were recorded and subtracted from the total number of MC.

From the analysis of the five 40x40 pixel boxes, a value was generated for mean number, size and integrated density (a product of the area and mean grey value) of GFP-MFAS aggregates for each box, the mean calculated for each gland and the data statistically analysed using GraphPad Prism. A Kruskal Wallis test was applied, followed by a Dunn's multiple comparisons post hoc test.

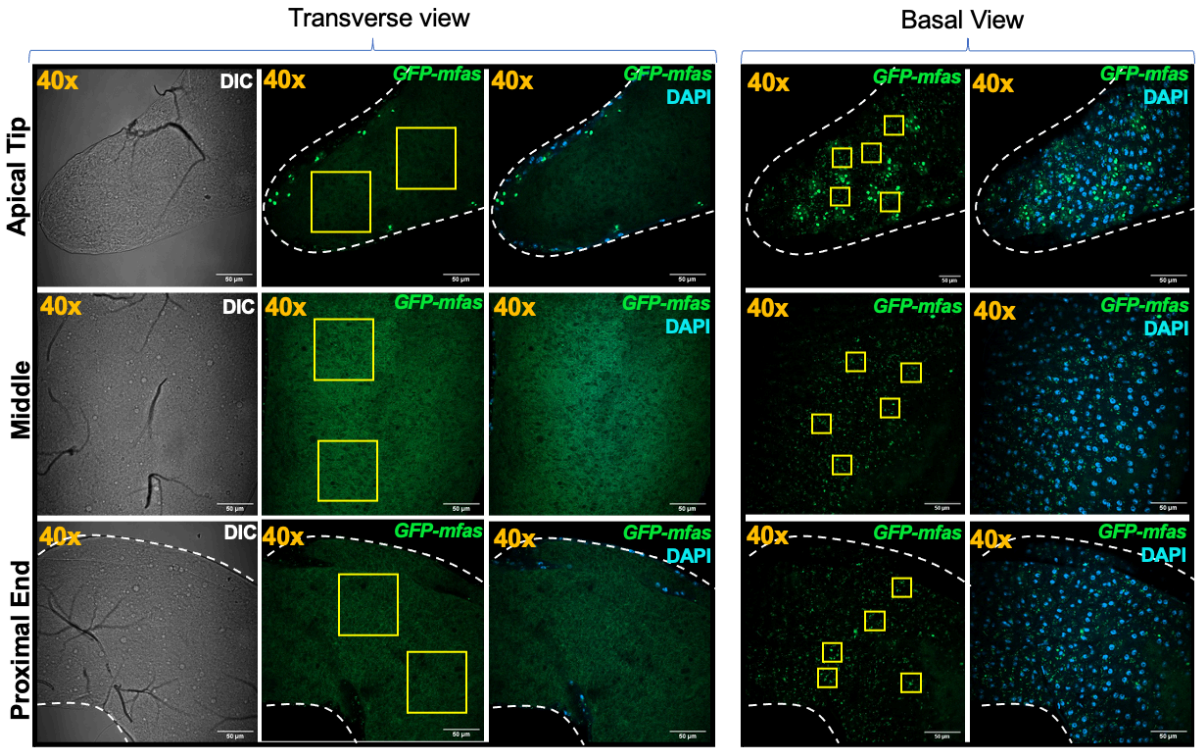

Figure 12: Image analysis technique.

Confocal micrographs (fluorescence or DIC) of 6-day-old virgin w^{1118} males expressing SC-specific *GFP-mfas* gene trap either alone or merged with DAPI or a single channel DIC. Two boxes x2 in the lumen of the gland in yellow represent those used to measure luminal intensity at the apical, middle and bottom of glands. Five boxes within the epithelium represent those used to calculate GFP-MFAS uptake.

Approximate gland boundaries are marked with a white dashed line. Scale bar = 50 μm.

3. Results

3.1 Mutant non-cleavable APPL expression in SCs induces abnormal propagation of DCG aggregating proteins to SCs

To investigate how APPL cleavage modulates the trafficking and uptake of GFP-MFAS in the accessory glands (AGs) of the male reproductive tract; I first overexpressed wild type and mutant-APPL in adult SCs under dsx-GAL4 controls, shown to induce abnormal uptake in neighbouring main cells (MCs) in the apical tip - extending this analysis to the middle and proximal ends of the AG. The APPL mutants [Appl-sd, Appl-sdΔE1], lacked α- and β-cleavage sites with the latter having an additional mutation in its E1 domain (**Figure 13B**).

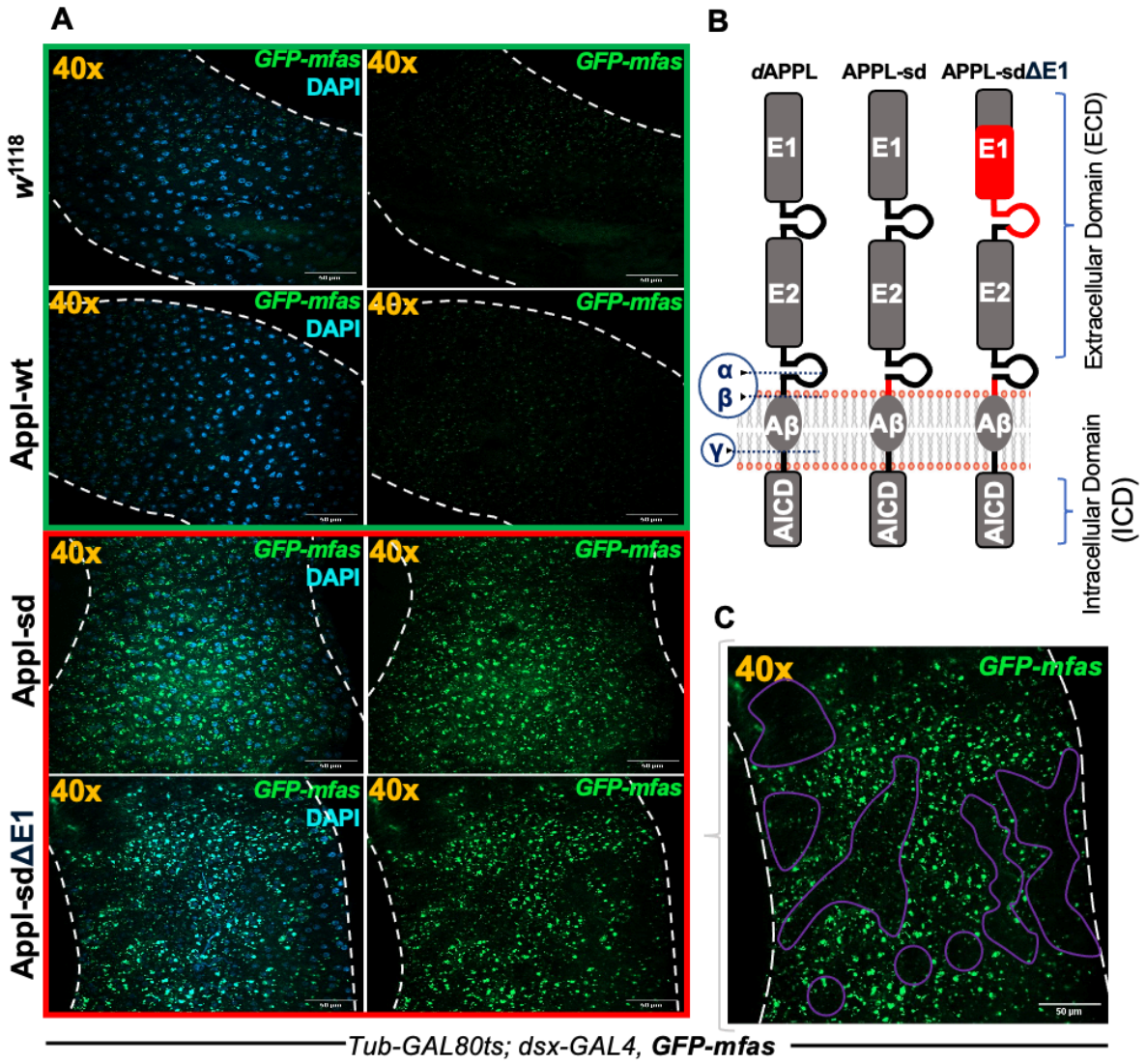

Figure 13: Expression of non-cleavable APPL mutants in SCs, induces the uptake of GFP-MFAS by MCs.

A. Confocal fluorescence basal-micrographs of the middle section 6-day-old virgin males expressing control APPL-wt, mutant APPL-sdΔE1 or APPL-sd or no Appl protein (w^{1118}) in addition to *GFP-mfas* gene trap, displayed either alone or in combination with a DAPI nuclear stain.
B. A schematic of full-length *Drosophila* APPL, with α-, β- and γ-cleavage sites identified, extracellular E1, and E2 domains, Aβ domain and amyloid precursor protein intracellular domain (AICD) labelled. APPL mutants APPL-sd and APPL-sdΔE1 are displayed alongside, with their deleted regions labelled in red.
C. Enlarged basal micrograph of middle section of AG in which APPL-sdΔE1 is expressed in SCs, with the areas of absent GFP-MFAS structures encircled in dark purple.

In all confocal images, approximate AG boundaries are marked by a dashed white line with 50 μm scale bars present in the bottom right corner.

To investigate the abnormal uptake phenotype previously reported [51] and its propagation through the AGs, I developed an analysis technique using ImageJ, placing five 40x40 pixel boxes, at the apical, middle and proximal ends of each AG to record an individual value for the mean number, size and integrated density of GFP-mfas fluorescent regions (called 'GFP-MFAS structures'). The box size was chosen for its capacity to fit between individual SCs clustered the tip of AG lobes.

Overexpressing the APPL mutants led to an accumulation of GFP-MFAS in enlarged compartments within MCs, throughout the AG body (apical tip, middle, and proximal ends), when compared with no-APPL and Appl-wt controls (**Figure 13A**), as measured by area of detectable fluorescence in MCs and integrated intensity (fluorescence intensity (mean grey value) x fluorescent area) (**Figures 14B-D**). However, the number of aggregates observed was generally unaffected or subtly altered by the different genetic manipulations, suggesting that the number of MFAS-containing lysosomal structures in MCs remains constant and is unchanged by APPL mutant expression in SCs. A "mosaic" pattern of GFP-MFAS-marked structures was also observed with mutant APPL overexpression (**Figures 13C, 14A**), which indicates that certain MC 'clusters' are more vulnerable to this pathology.

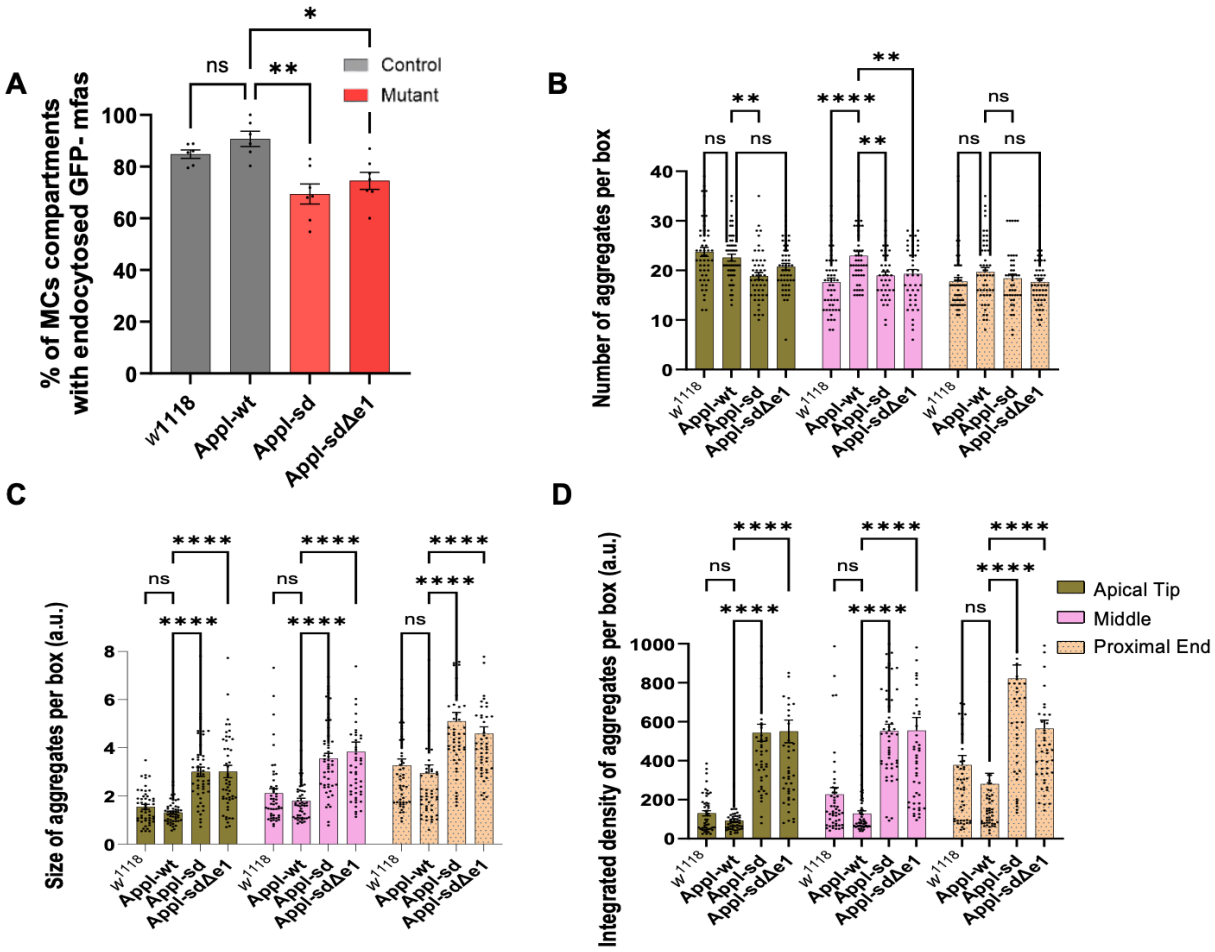

Figure 14: Expressing APPL-mutants in SCs induces abnormal propagation of DCG aggregating proteins to MCs, located throughout the whole AG body.

A. Bar chart displaying the % area of MCs with the endocytosed GFP-MFAS. N (number of midline glands) = w^{1118} - 6, Appl-wt – 6 , Appl-sd – 7, Appl-sdΔE1 - 7.

B-D Bar charts comparing the mean number, size and intensity (integrated density) of GFP-MFAS structures per box in the apical tip (green), middle (pink) and proximal (orange) of AGs for each genotype. N (number of AGs) = w^{1118} - 10, Appl-wt - 10, Appl-sd – 10, Appl-sdΔE1 - 10.

In bar charts, bar heights represent the group mean, with error bars corresponding to the ± standard error of the mean (SEM). Individual data points (black dots) represent the mean number, size, or integrated density of aggregates in each 40x40 pixel sample box. Graphs were analysed using a Kruskal-Wallace, followed by a Dunn's multiple comparisons post hoc test. The degrees of significance are indicated as follows: *P < 0.05, ***P < 0.001, ****P < 0.0001 and ns as non-significant.

3.2 Expression of human wild type and mutant Aβ in SCs induces abnormal propagation of DCG aggregating proteins to MCs

Having validated the ability of SC-expressed mutant APPL to induce an abnormal phenotype in MCs, I tested whether these APPL-dependent effects may also be influenced by expression

in SCs of the wild type and mutants in the amyloidogenic $A\beta_{42}$ region of human APP (**Figure 15B)**, which have been proposed to mediate its pathological effects via human APP [67]. Previous experiments have suggested mutant Aβ expression in SCs induced uptake of GFP-MFAS by MCs at the apical tip of the accessory gland [1]. To investigate this further, I overexpressed three pathological familial Aβ-mutants in SCs: Arctic [68], Dutch [51, 69], and Iowa [70], alongside controls (the wild-type form of the $A\beta_{42}$ peptide, Aβ-wt, and no $A\beta_{42}$ (w^{1118}) expression [51]). These three clinical Aβ mutants have been studied extensively within humans and mice models, each having unique stereochemical characteristics and aggregation kinetics and are all associated with increased intracellular toxicity and resistance to degradation [68, 71-73] when compared to Aβ-wt controls. In *Drosophila*, expressing $A\beta_{42}$ mutants within the nervous system incudes neurotoxicity and cell death across neuronal cell types [74]. These mutants generate peptide variants with distinct aggregation propensities both qualitatively and quantitatively modifying their pathology *in vivo*, corresponding with their distinct neurodegenerative patterns seen in human fAD patients [75, 76].

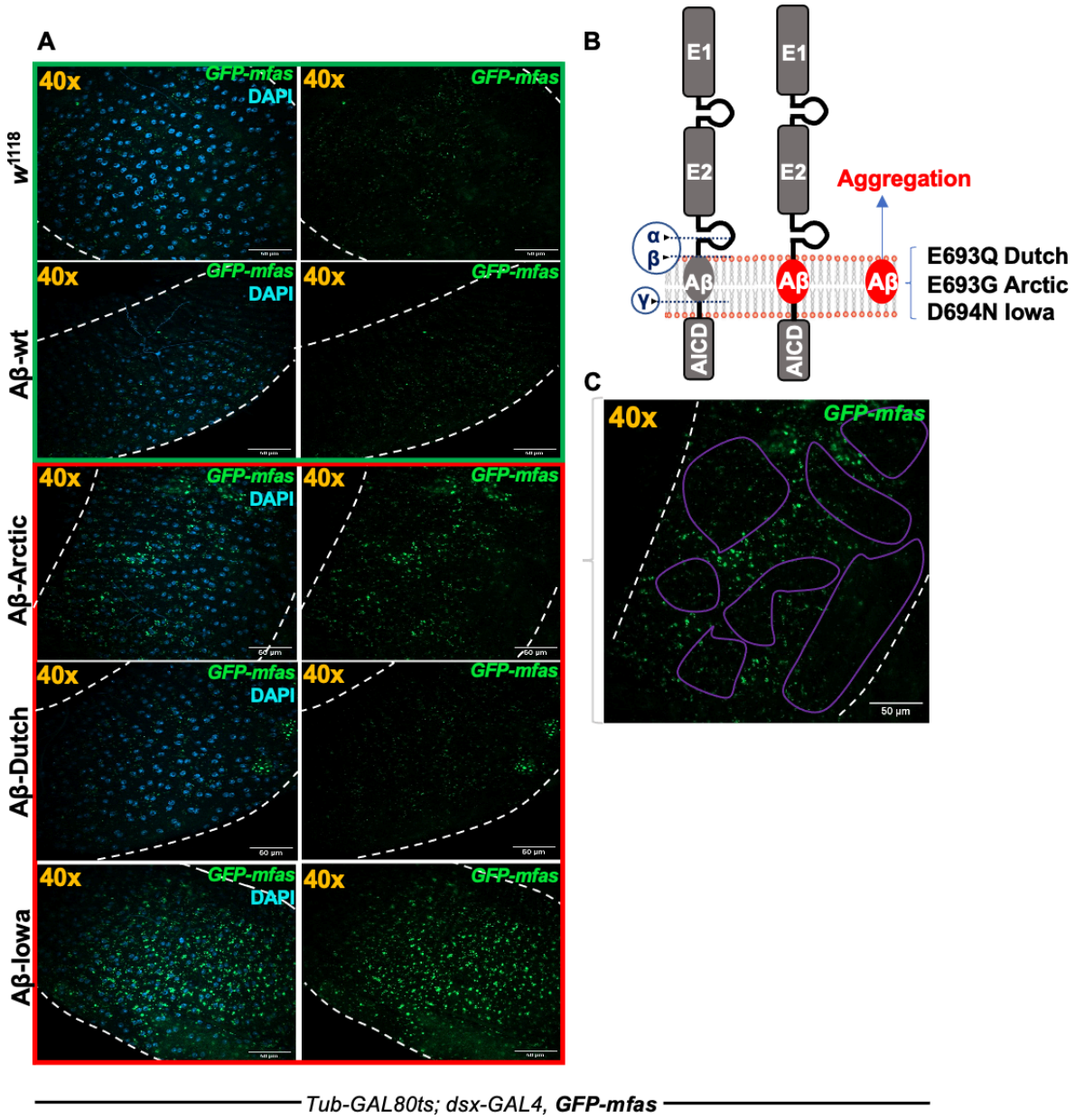

Figure 15: Expression of pathological mutant Aβ$_{42}$ peptides induces abnormal propagation of DCG aggregating proteins to MCs.

A. Confocal fluorescence basal micrographs of 6-day-old virgin males expressing Aβ-mutants: Arctic, Iowa, and Dutch boxed in red alongside *w^{1118}* and Aβ$_{42}$-controls, in green, in AGs, displayed with SC-specific *GFP-mfas* gene trap alone or merged with DAPI.
B. Schematic displaying Drosophila APPL (left) and human APP (middle), α-, β- and γ-cleavage sites identified, extracellular E1, and E2 domains, Aβ domain and amyloid precursor protein intracellular domain (AICD) labelled. Illustrated alongside are Aβ$_{42}$ mutants: Dutch, Arctic, and Iowa highlighted red, shown to induce aberrant aggregation.
C. Enlarged midline basal image of Aβ-Arctic with the areas of absent GFP-MFAS endocytosis encircled in dark purple.

In all confocal images, approximate AG boundaries are marked by a dashed white line with 50 µm scale bars present in the bottom right corner.

Expression of Aβ-mutants Iowa and Arctic in flies resulted in a selective increase in the size and integrated intensity of GFP-MFAS lysosomal structures in MCs in comparison with w^{1118} (no-Aβ) and Aβ-wt controls (**Figures 16C, D**) With often minor and non-significant reductions in the number of these structures (**Figure 16B**). Uptake of GFP-MFAS by MCs in Aβ-mutant-expressing AGs was also mosaic, mirroring the phenotype observed in APPL mutants (**Figures 15C, 16A**).

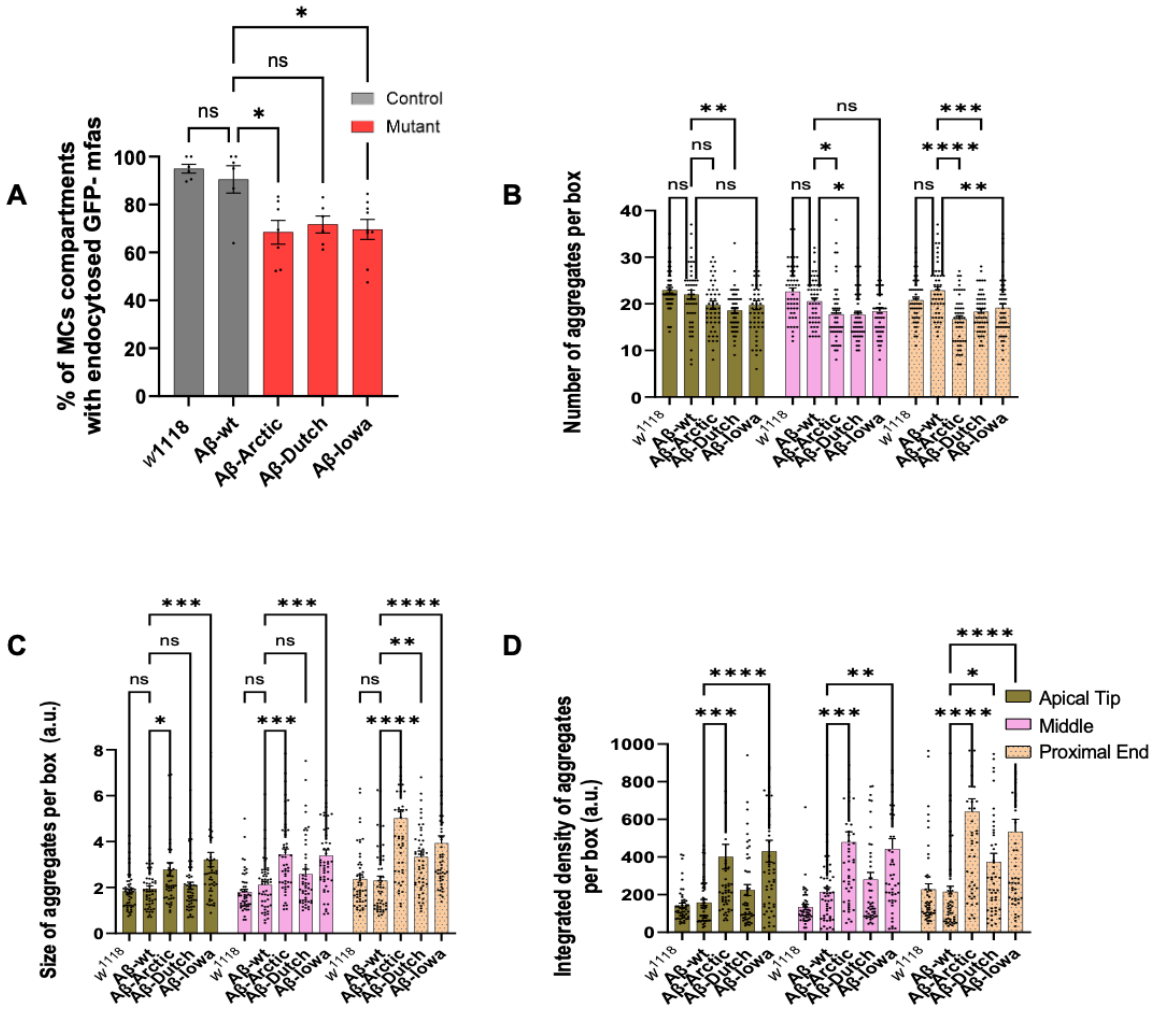

Figure 16: Expression of pathological mutant Aβ$_{42}$ peptides induces abnormal propagation of GFP-MFAS to vulnerable MCs present through the whole AG body.

A. Bar graph displaying the %. Of MCs with the endocytosed GFP-MFAS present within their lysosomal compartments. N = N (number of AGs) = w^{1118} - 6, Aβ-wt - 6, Aβ-Arctic – 7, Aβ-Dutch – 6, Aβ-Iowa – 9.

B-D Bar charts comparing the mean number, size and intensity (integrated density) of aggregates per box in each location in the gland for different genotypes. N (number of AGs) = w^{1118} - 10, Aβ-wt - 10, Aβ-Arctic – 10, Aβ-Dutch – 10, Aβ-Iowa – 10.

In bar charts, bar heights represent the group mean, with error bars corresponding to the ± standard error of the mean (SEM). Individual data points (black dots) represent the mean number, size, or integrated density of aggregates in each 40x40 pixel sample box. Graphs were analysed using a Kruskal-Wallace, followed by a Dunn's multiple comparisons post hoc test. The degrees of significance are indicated as follows: *P < 0.05, ***P < 0.001, ****P < 0.0001 and ns as non-significant.

The MC uptake phenotypes analysed above emerge in AGs during the six-day period following adult exclusion. During this time MCs mature and secrete a complex cocktail of SFPs, stimulating the AG lumen to expand rapidly and compressing MCs against the outer muscular sheath of the gland. Concurrently, secondary cells form mature DCG compartments that release their contents into the AG lumen [77].

The uptake of GFP-MFAS by MCs throughout the gland in wild type animals and also in animals expressing mutant APPL and Aβ-peptides in SCs strongly suggests that MCs are endocytosing this secreted material. In glands with APPL and $A\beta_{42}$ mutant-expressing SCs, DCG maturation is disrupted, and this presumably affects the properties of secretions, leading to GFP-MFAS being preferentially endocytosed from the accessory gland lumen by non-expressing MCs or suppressing the breakdown of this endocytosed material in MC lysosomes, or both (see also [51]).

3.3 Endocytosed GFP-MFAS in MCs is usually secreted and gradually re-endocytosed following mating, but mutant APPL and Aβ expression in SCs affects this process

SCs maintain a basal level of DCG secretion and constitutively generate new DCG compartments in virgin males [59]. Mating stimulates the rapid ejection of seminal fluid proteins (SFPs) into the female reproductive tract (FRT), and the rapid compensatory release

of ~3-4 SC DCG compartments from each SC accelerating luminal content replenishment [59]. These DCGs are rapidly replenished under autocrine BMP-dependent signalling control. I investigated the effects of SC-expressed non-cleavable APPL and $A\beta_{42}$ mutants, which disrupt the formation of DCGs, on the fate of DCG-derived proteins internalized by MCs during post-mating recovery -- a process critical to restoring gland homeostasis in preparation for subsequent remating.

GFP-MFAS was rapidly released from MCs during mating in the absence and presence of wild type APPL overexpression in SCs **(Figures. 17 and 18B, C**). There was potentially some re-endocytosis by MCs in the following three hours, through these changes were not significant (**Figure 18B**). I hypothesised that lysosomal compartments produced by uptake of GFP-MFAS secretion following expression of mutant APPL proteins in SCs might also be rapidly released and re-endocytosed following mating. Indeed, by assessing changes in integrated fluorescence intensity, I found that GFP-MFAS was rapidly secreted, but there was an increased level of reuptake over the following three hours in APPL-mutants (**Figure 18C**).

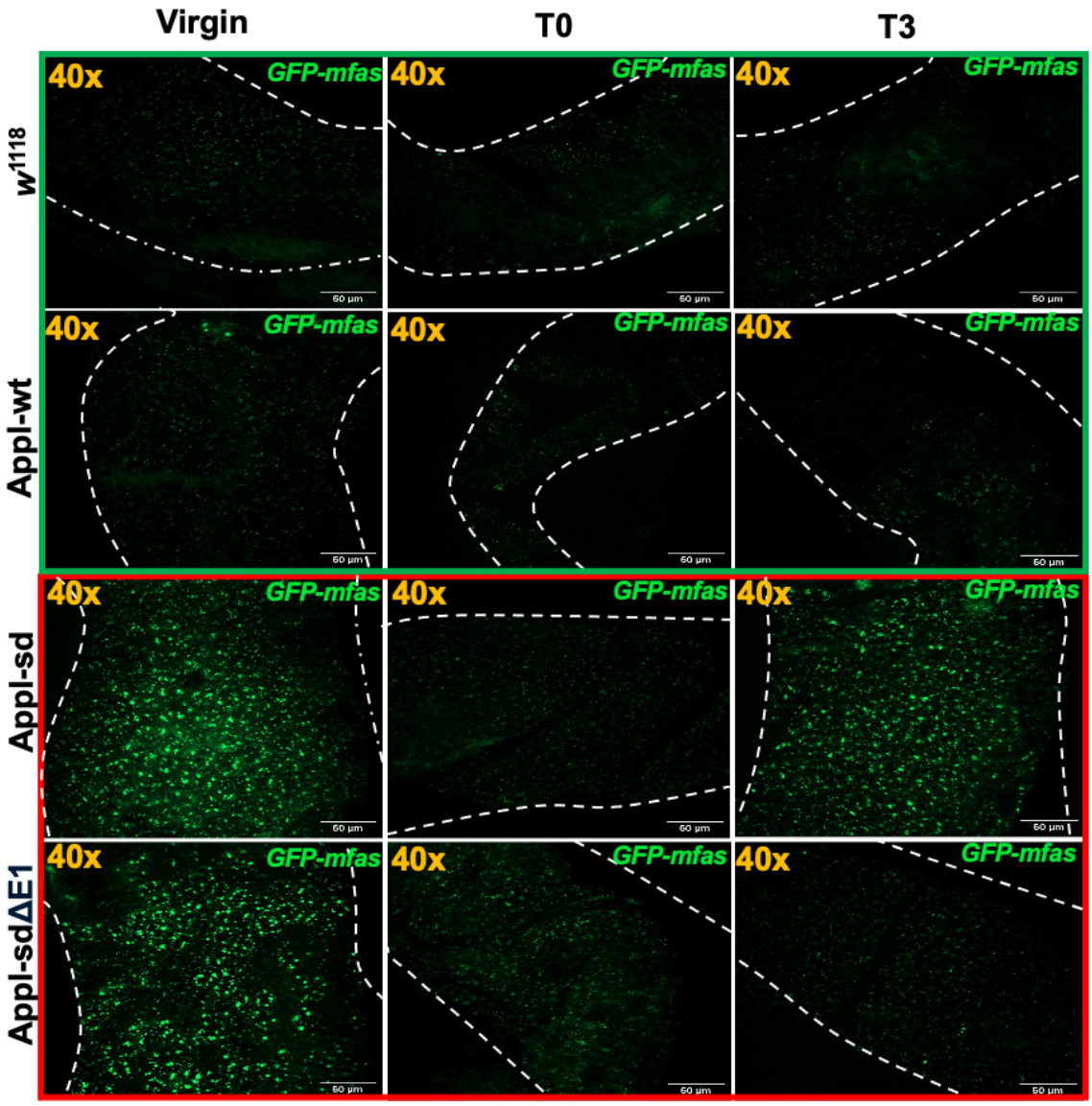

Figure 17: Lysosomal GFP-MFAS is partially ejected from MCs of virgin AGs upon mating and is then re-endocytosed in controls and glands with SC-specific APPL-mutant expression.

Confocal fluorescence micrographs, displaying the middle of AGs - from virgin, and time zero, and three-hours post-mating. Appl-sd, Appl-sdΔE1 expressed in SCs (red box) below w^{1118}, and Appl-wt (green box).

In all confocal images, approximate AG boundaries are marked by a dashed white line with 50 µm scale bars present in the bottom right corner.

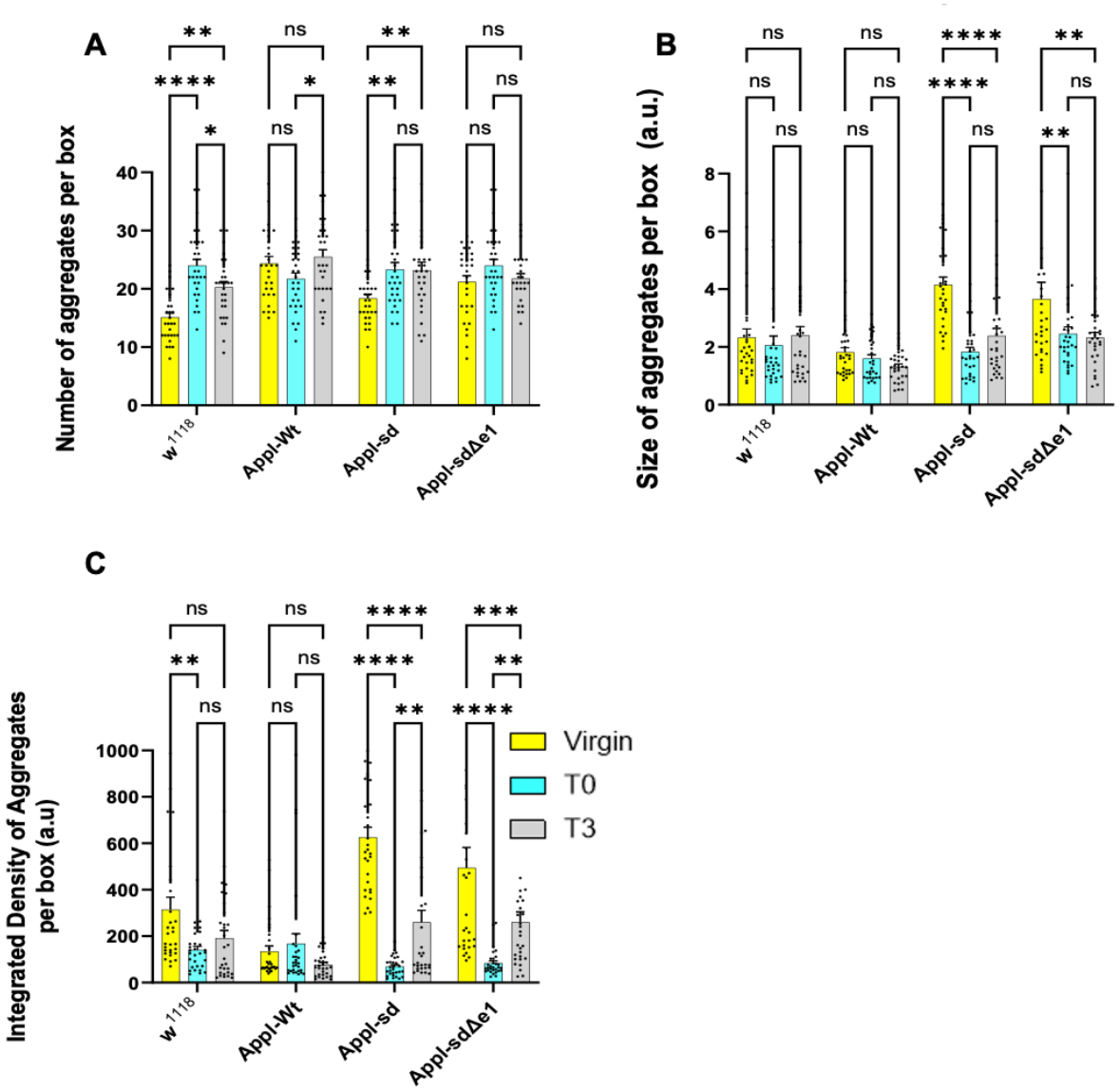

Figure 18: Lysosomal GFP-MFAS is ejected from MCs of virgin AGs upon mating, while MC lysosomal compartments are reformed more rapidly when mutant APPL proteins are expressed in SCs.

A-C Bar charts comparing the mean number, size and intensity (integrated density) of aggregates per box at the middle of AGs from virgin, zero, and three-hours post-mating males, and changes compared over the time-course. N (Number of AGs), for virgin, T0 and T3 experiments: = w^{1118} - 6, Appl-wt - 6, Appl-sd – 6, Appl-sdΔE1 - 6.

In bar charts, bar heights represent the group mean, with error bars corresponding to the ± standard error of the mean (SEM). Individual data points (black dots) represent the mean number, size, or integrated density of aggregates in each 40x40 pixel sample box. Graphs were analysed using a Kruskal-Wallace, followed by a Dunn's multiple comparisons post hoc test. The degrees of significance are indicated as follows: *P < 0.05, ***P < 0.001, ****P < 0.0001 and ns as non-significant.

I also investigated whether this rapid release and partial re-uptake following mating was observed when human Aβ-mutants, which induce increased uptake of GFP-MFAS by MCs, were expressed in SCs (**Figure 19**). My results revealed that when Aβ-mutants were overexpressed in SCs, each mutant induced different release and re-uptake phenotypes (**Figure 19**). For Dutch and Iowa Aβ-mutants, a significant proportion of the endocytosed GFP-MFAS was released upon mating, but only MCs in glands expressing the Iowa mutant showed significant re-uptake over the next three hours (**Figures 20B, C**). By contrast, when SCs expressed the Arctic mutant, there was no significant release of GFP-MFAS from MCs (**Figure 20B**). The results with Aβ-wild type-expressing SCs, where MCs endocytose levels of GFP-MFAS similar to non-expressing control glands, were less conclusive. Some GFP-MFAS did appear to be released, but it was not taken up again.

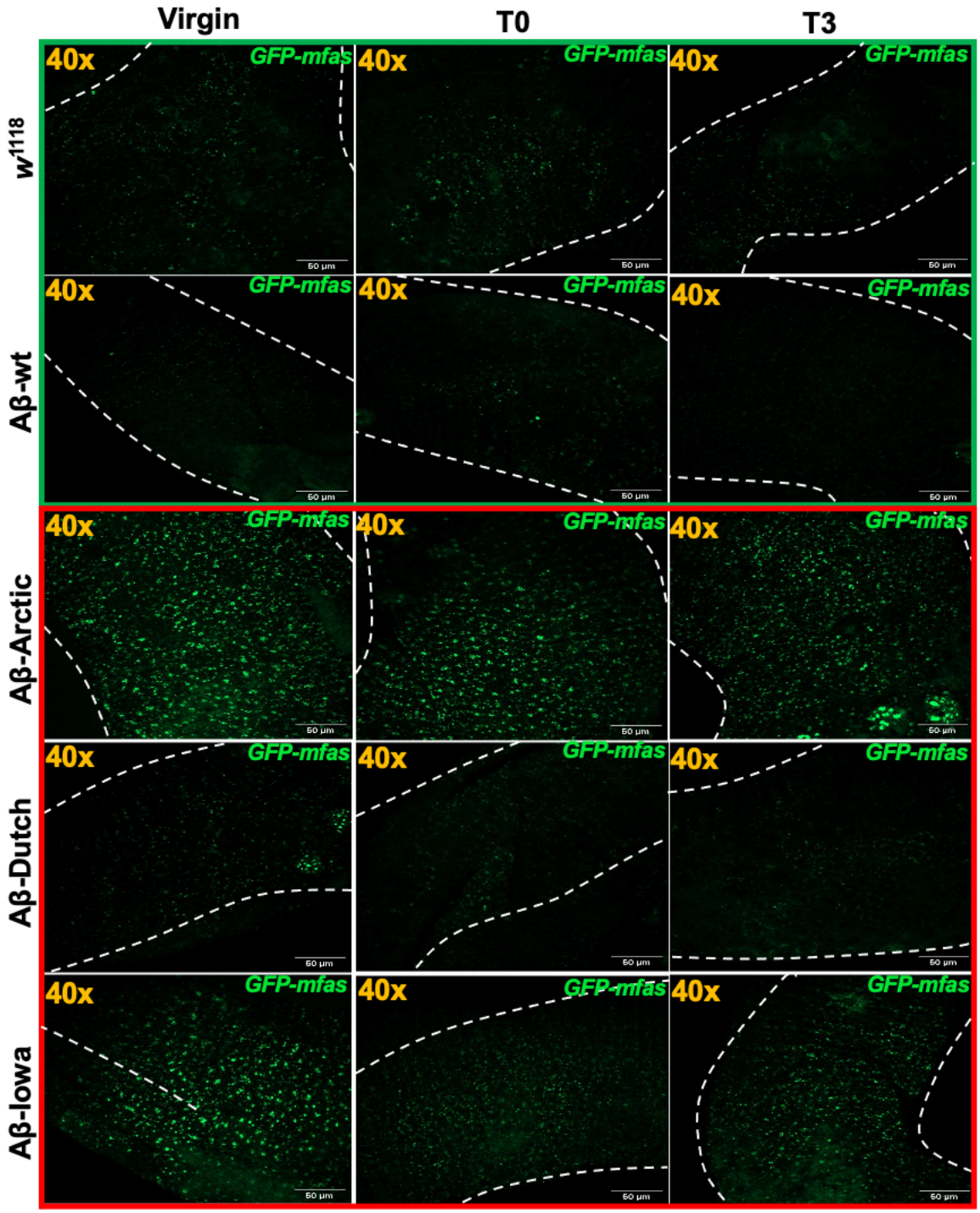

Figure 19: Expressing Aβ-mutant peptides in some cases ejects GFP-MFAS from MCs of virgin AGs upon mating and is subsequently re-endocytosed in different patterns post-mating.

Confocal fluorescence micrographs, displaying the middle of AGs expressing *GFP-mfas* gene trap from virgin, and zero, and three-hours post-mating males. In these AGs from 6-day-old male flies, images of glands expressing SC-specific Arctic, Iowa and Dutch Aβ-mutants are boxed in red, alongside w^{1118} and $A\beta_{42}$-controls in green.

In all confocal images, approximate AG boundaries are marked by a dashed white line with 50 µm scale bars present in the bottom right corner.

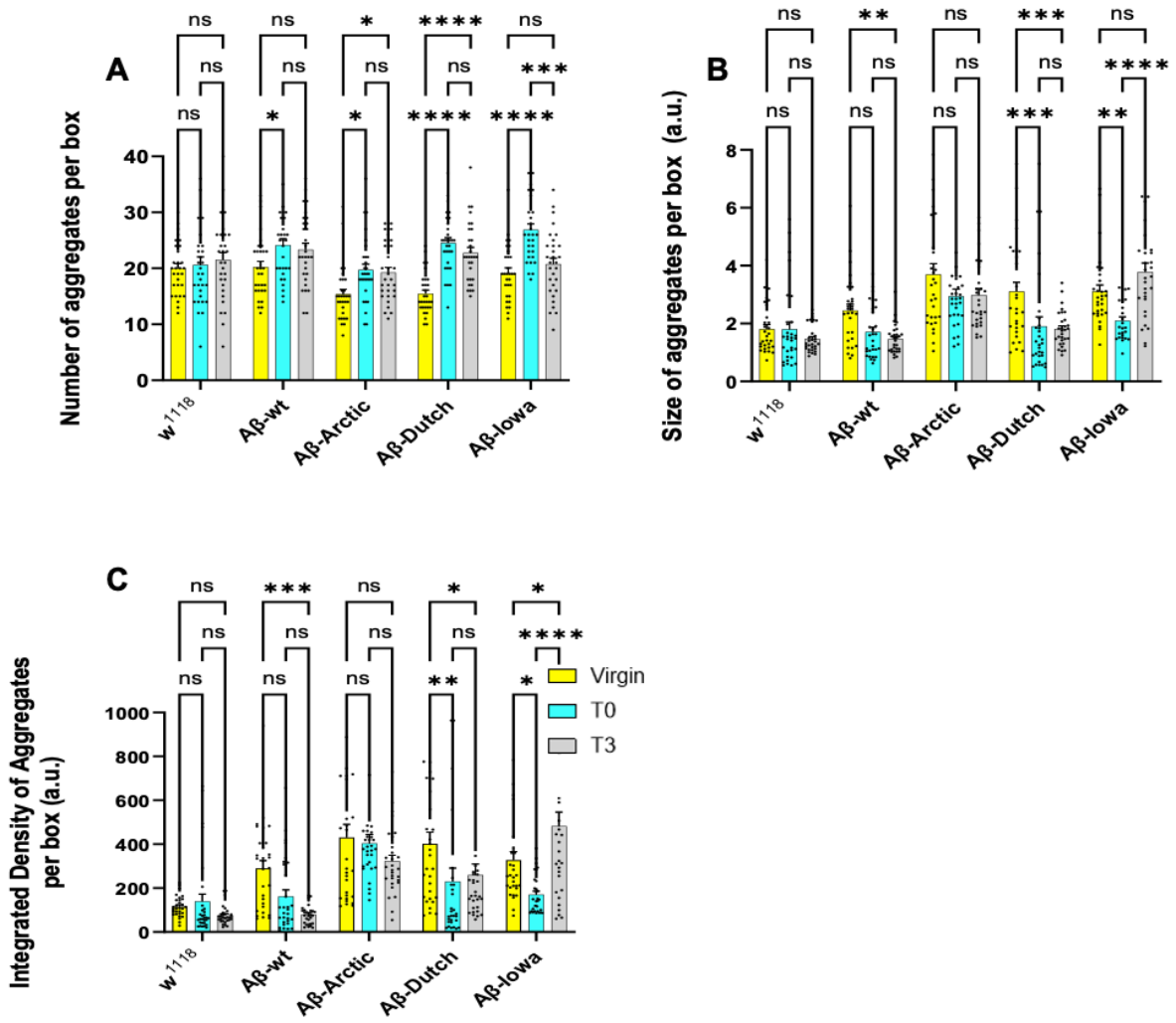

Figure 20: Expressing Aβ-mutant peptides, induces the post-mating reformation of lysosomal compartments in a manner that differs between individual mutants.

A-C Bar charts comparing the mean number, size and intensity (integrated density) of aggregates per box at the middle of AGs from virgin, zero, and three-hours post-mating males in which SCs are expressing Arctic, Iowa and Dutch Aβ-mutants, wt-Aβ or no Aβ. N (Number of glands), for virgin, T0 and T3 experiments: w1118 - 6, Aβ-wt - 6, Aβ-Arctic – 6, Aβ-Dutch – 6, Aβ-Arctic – 6.

In bar charts, bar heights represent the group mean, with error bars corresponding to the ± standard error of the mean (SEM). Individual data points (black dots) represent the mean number, size, or integrated density of aggregates in each 40x40 pixel sample box. Graphs were analysed using a Kruskal-Wallace, followed by a Dunn's multiple comparisons post hoc test. The degrees of significance are indicated as follows: *P < 0.05, ***P < 0.001, ****P < 0.0001 and ns as non-significant.

3.4 Secretion from Appl-sdΔE1-expressing SCs is required to induce the pathological spread in MCs

To investigate the mechanisms underlying the abnormal transfer of secreted SC GFP-MFAS to MCs, I focused on the effects of APPL-sdΔE1, which gives a particularly strong propagation phenotype.

To confirm that apical secretions of GFP-MFAS from SCs are required to propagate the abnormal pathology induced in MCs, a stable line expressing the *GFP-mfas* gene trap and *Appl-sdΔE1* under GAL4/UAS control was constructed by Bhavna Verma, producing a stock that generated a strong endocytic MC-phenotype at temperatures permissive for Appl-sdΔE1 expression (29^{o}C). In these conditions, Appl-sdΔE1 mutant protein generated a unique GFP-MFAS aggregated network phenotype inside SC DCG compartments, with GFP-MFAS intricately lining the periphery of the compartments [51]. These compartments were acidified and apparently targeted for lysosomal degradation, but ultimately appeared to be secreted [51]. We hypothesised that suppressing SC secretion through the regulated secretory pathway might suppress the abnormal endocytic pathology in MCs. Autocrine BMP signalling has previously been shown to stimulate DCG compartment biogenesis in SCs in response to the release of BMP ligand Decapentaplegic (DPP) from DCG compartments [59].

Overexpressing the transcriptional repressor of BMP signalling, DAD or RNAi targeting *Dpp* significantly reduced the levels of GFP-MFAS in the lumen of the AG (**Figures 21A, B**) and also reduced abnormal transfer of the GFP-MFAS into MCs (**Figures 21A, C-E**), strongly indicating that this material is taken up from the luminal content of the AG, which includes SC secretions.

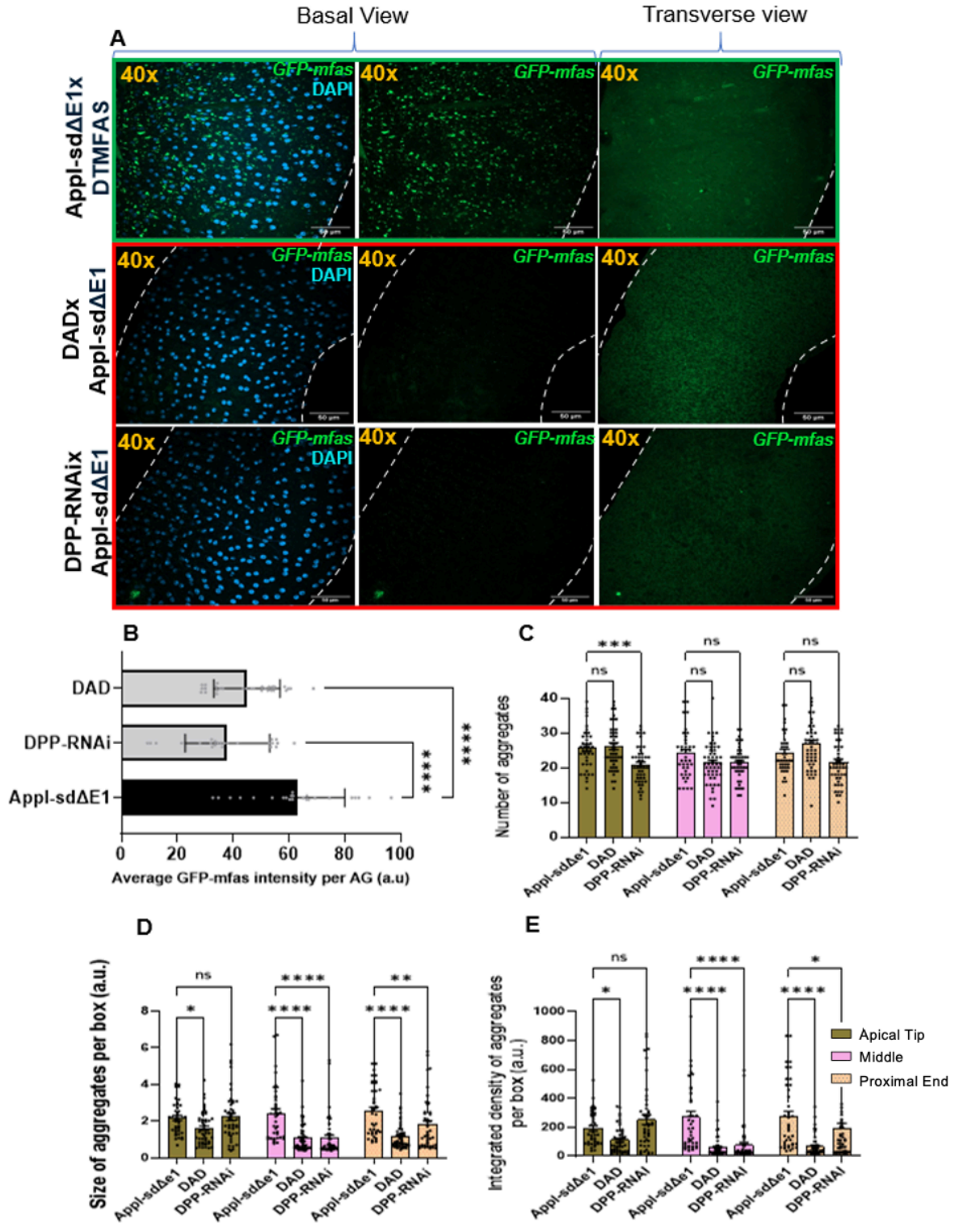

Figure 21: SC secretions are required to transfer Appl-sdΔE1 abnormal pathology into MCs.

A. Fluorescence micrographs of fixed virgin male accessory glands expressing SC-specific *GFP-mfas* gene trap. Images show AG epithelia (first and second columns) and the AG lumen (final column) under different genetic conditions: *Appl-sdΔE1* x DTMFAS alone or in combination with *UAS-Dad* and *UAS-DPP-RNAi*.

B. Bar chart showing quantification of the GFP intensity in the accessory gland lumen for the three genotypes. N (number of AGs) = Appl-sdΔE1 - 10, DAD - 10, DPP – 10.

C-E Bar graphs comparing the mean number, size, and integrated density of GFP-positive aggregates across different regions of the AG epithelium (apical tip, middle, and proximal ends) for the indicated genotypes. N (number of AGs) = Appl-sdΔE1 – 10, DAD – 10, DPP – 10.

In all confocal images, approximate AG boundaries are marked by a dashed white line with 50 μm scale bars present in the bottom right corner. In bar charts, bar heights represent the group mean, with error bars corresponding to the ± standard error of the mean (SEM). Individual data points (black dots) represent the mean number, size, or integrated density of aggregates in each 40x40 pixel sample box. Graphs were analysed using a Kruskal-Wallace, followed by a Dunn's multiple comparisons post hoc test. The degrees of significance are indicated as follows: *P < 0.05, ***P < 0.001, ****P < 0.0001 and ns as non-significant.

3.5 Exosome biogenesis is required for generation of the Appl-sdΔE1-induced endolysosomal defect in MCs.

Singh et al, 2024, postulated that expression of non-cleavable APPL mutants or mutant Aβ-peptides in SCs affects the dissociation of DCG protein aggregates from the membranes of the Rab11-positive secretory compartments and ILVs inside them that initially prime aggregation. Our group has previously shown that Rab11-exosomes generated in these compartments require a group of accessory ESCRT-III proteins for their formation, which are not needed for exosome biogenesis in late endosomal compartments [63]. Knockdown of *Chmp5*, an accessory ESCRT-III protein, in SCs inhibits Rab11-ILV formation and exosome-mediated female behavioural responses. Knockdown of *Chmp5* in human colorectal HCT116 cells has been shown to inhibit Amphiregulin-mediated cancer exosome signalling and leads to a selective reduction in the Rab11a marker in small EV (sEV) preparations [63].

In addition, GAPDH2 exhibits a 'moonlighting' function in clustering ILVs within Rab11-positive DCG compartments and also clusters other secreted extracellular vesicles [78]. Other work by the Wilson group has suggested an evolutionary conserved association between GAPDH2 and Rab11-exosomes as studies in sEV preparations from human cancer cells enriched with Rab11-exosomes show an increased level of EV-associated GAPDH, as well as Rab11a [51].

Based on these findings, I hypothesised that the association between Rab11-exosomes and DCG aggregates might be important in endocytic uptake of these aggregating proteins by MCs, which would therefore be blocked by suppressing Rab11-exosome production. We also decided to test whether GAPDH2 might be involved in exosome-aggregate interactions, influencing the transfer of GFP-MFAS protein.

Neither *Chmp5-RNAi*, nor *GAPDH2-RNAi* knockdown significantly reduced the level of GFP-MFAS secretion into the AG lumen (**Figures 22A, B**). However, the abnormal transfer of GFP-MFAS into MCs induced by expression of Appl-sdΔE1 was strongly suppressed by *Chmp5-RNAi* but not by GAPDH2 knockdown (**Figures 22A, C-E**). Surprisingly, GAPDH2 knockdown did produce a small, but significant, decrease in the number of total lysosomal structures in MCs versus controls, suggesting that loss of its vesicle-clustering activity may have an effect on the number of MCs that endocytoses GFP-MFAS.

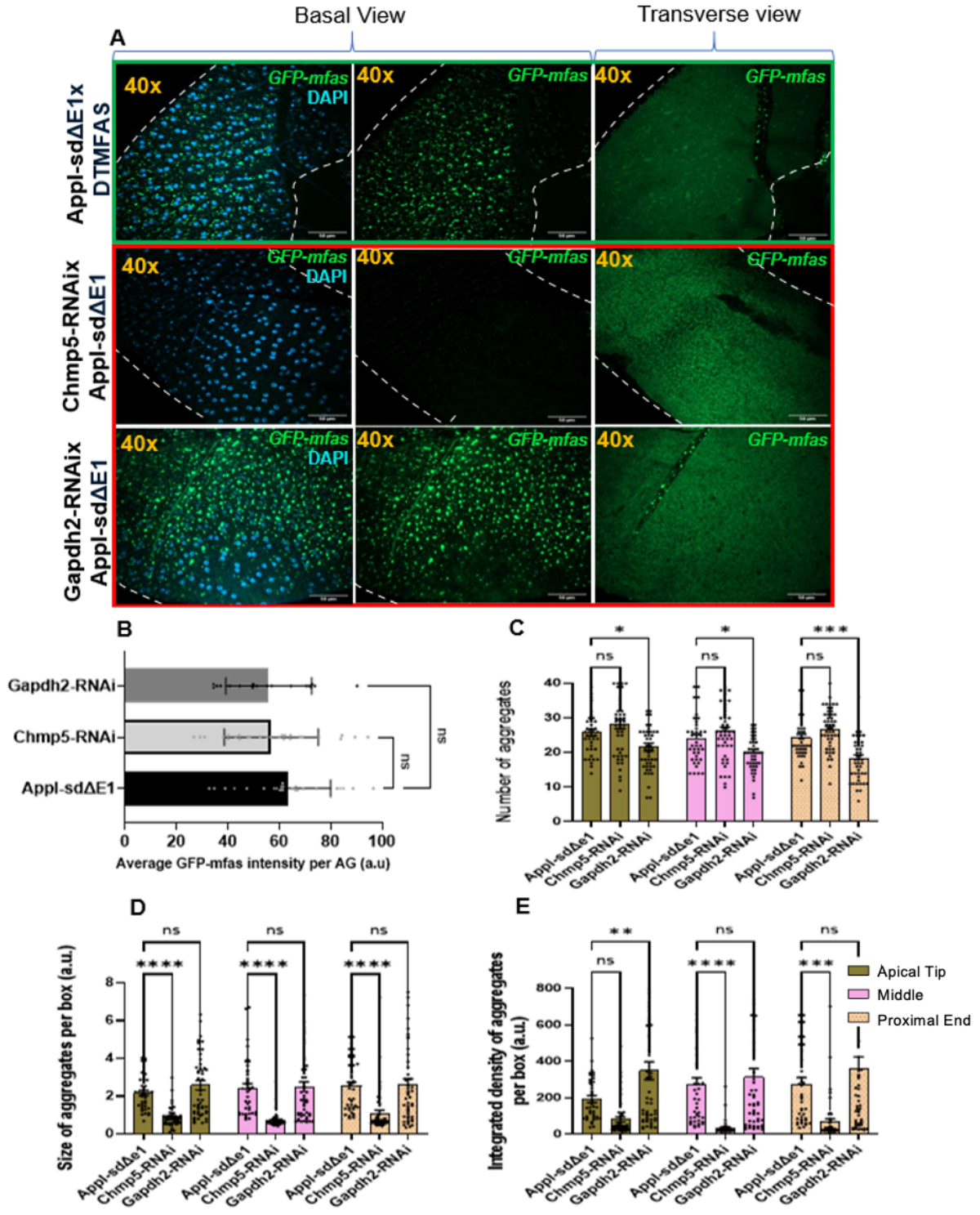

Figure 22: Exosome biogenesis and not ILV clustering is required for the abnormal transfer of GFP-MFAS to MCs from Appl-sdΔE1-expressing SC, but neither is required for GFP-MFAS secretion.

A. Fluorescence micrographs of the middle of fixed virgin male AGs expressing SC-specific *GFP-mfas* gene trap alongside GAL4-UAS-driven SC Appl-sdΔE1 either alone or in combination with

GAPDH2-RNAi or *Chmp5-RNAi*. Images show AG epithelia (first and second columns) and the AG lumen (third column).

B. Bar graph quantifying the average GFP intensity in the AG lumen across the three recombinant genotypes. N (number of AGs, virgin and mated) = Appl-sdΔE1 = 10, Chmp5 = 9, GAPDH2 = 8.

C-E Bar graphs comparing the mean number, size, and integrated density of GFP-positive aggregates across different regions of the AG epithelium (apical tip, middle, and proximal ends) for the indicated genotypes. N (number of AGs) = Appl-sdΔE1 = 10, Chmp5 = 9, GAPDH2 = 8.

In all confocal images, approximate AG boundaries are marked by a dashed white line with 50 μm scale bars present in the bottom right corner. In bar charts, bar heights represent the group mean, with error bars corresponding to the ± standard error of the mean (SEM). Individual data points (black dots) represent the mean number, size, or integrated density of aggregates in each 40x40 pixel sample box. Graphs were analysed using a Kruskal-Wallace, followed by a Dunn's multiple comparisons post hoc test. The degrees of significance are indicated as follows: *P < 0.05, ***P < 0.001, ****P < 0.0001 and ns as non-significant.

4. Discussion

Emerging research suggests that APP, its cleavage products and other amyloidogenic proteins have complex and often interlinked roles that regulate a wide-range physiological functions – regulating their own trafficking, processing, secretion and signalling effects [46, 51]. In AD, defects in this multi-layered network result in protein misfolding and accumulation in specific brain regions, following a distinct spatial pattern [21, 22]. However, despite intensive research efforts, unravelling the mechanisms underlying the initial stages of the disease onset remain difficult, often hindered by the disease's molecular complexity, decades-long development, and heterogeneity of pathological symptoms.

To address these challenges, the Wilson group has pioneered a novel prostate-like secondary cell system within *Drosophila melanogaster* to model early-stage AD. Building on this work, my findings demonstrate that expression of non-cleavable forms of APPL, the fly APP homologue, or overexpressing humanised $A\beta_{42}$ mutants induces the formation of an abnormal uptake phenotype. In this phenotype GFP-MFAS, a major component of the DCGs, is preferentially endocytosed by vulnerable main cells, leading to the formation of aggregated deposits resistant to lysosomal degradation. Notably, this phenotype extends throughout the whole AG body, correlating with potentially pathological changes in the endolysosomal system - mirroring early AD-associated pathologies commonly observed intra-neuronally [79].

In studying the secretory mechanisms of SCs expressing the APPL-sdΔE1 mutant protein, I found that suppressing proteins required for adult BMP-stimulated SC growth and secretion, or overexpressing a negative regulator of BMP signalling [59] blocked endocytic transfer of GFP-MFAS. In addition, by inducing an RNAi knockdown of *Chmp5,* a specific regulator of Rab11-exosome production [63], I observed that the transfer phenotype was also suppressed without affecting secretion of GFP-MFAS by SCs [63], suggesting that this process is dependent on Rab11-exosomes.

4.1 Overexpressing APP mutants that affect protein aggregation events in the DCG alters the properties of secreted GFP-mfas, enabling its uptake by MCs

Transmembrane APPL localizes to DCG limiting membranes, where it interacts directly or indirectly with the TGFBI homologue MFAS to drive SC protein aggregation events critical for DCG maturation [51].

In SCs, I expressed two non-cleavable APPL mutants, APPL-sd and APPL-sdΔE1 [51, 79] both lacking α- and β-secretase cleavage sites. The extracellular domain of these mutants cannot detach from the limiting membranes of secretory compartments or ILV-limiting membranes during DCG maturation, impairing membrane detachment of aggregated GFP-MFAS within DCG structures. Notably, APPL-sdΔE1, which appears to exhibit a stronger membrane association, induces a unique peripheral aggregated network phenotype in DCG compartments [51]. The deleted E1 domain contains growth factor-like domain (GFLD) and a copper-binding domain (CuBD) which mediates divalent cation-dependent APP dimerization. In neurodegenerative diseases, dysregulation of this bi-directional dimerization is strongly associated with pathological protein aggregation and synaptic dysfunction in both humans [80, 81] and *Drosophila* [82, 83].

My data demonstrates that the expression of APPL mutants significantly alters uptake of secreted GFP-MFAS, enhancing its accumulation in lysosomal compartments of MCs. Importantly, this uptake phenotype was not only restricted to MCs at the AG's apical tip, which had previously been observed [51], but was also distributed throughout the entire gland (**Figure 14**). Furthermore, once the stored GFP-MFAS is ejected upon mating, it is subsequently re-endocytosed post-mating at rates comparable to controls (**Figure 18**). However, the properties of this re-endocytosed GFP-MFAS differ between APPL mutants and controls, as the former generates MFAS structures that more rapidly reform within lysosomal compartments (**Figure 18C**).

The pattern of GFP-MFAS uptake by MCs may provide further insight into mechanisms of intraneuronal Aβ deposition, as single nucleotide-RNA (snRNA-seq) studies have revealed that subcellular heterogeneity across neuronal subtypes is greatly correlated with Aβ-plaque burden [84, 85]. In AGs, recent single-cell transcriptomic analysis has hypothesised the presence of two distinct MC subtypes [86]. My findings are consistent with this model, indicating that one MC subtype, which may be characterised by factors such as an elevated metabolic activity and/ or expression of specific genes, may be more prone to GFP-MFAS accumulation, while the other subtype remains comparatively unaffected (**Figures 13C, 14A**). This selective vulnerability may reflect inherent characteristics underlying neuronal susceptibility in Alzheimer's disease pathology and provides a broader framework for understanding how differences in cellular state contribute to disease-associated protein accumulation.

4.2 Pathogenic Aβ Mutations Disrupt Secretory Trafficking and Recapitulate AD-Associated Endolysosomal Dysfunction

Expression of $A\beta_{42}$ mutant peptides in SC secretory compartments drives the abnormal endocytosis of GFP-MFAS by MCs from the AG lumen, mirroring the endocytic defects observed with APPL mutants. Among these, the Arctic (APP E693G; $A\beta_{42}$ E22G) and Iowa (APP D693N; $A\beta_{42}$ D23N) mutants induced the most severe phenotype in MCs, consistent with their ability to direct the reorganization of GFP-MFAS aggregation in SCs [51].

The mutant Aβ-Arctic peptide is associated with an increased propensity to form protofibril-aggregates during fibril biogenesis [87], resulting from its ability to form more densely packed protofilament-protofilament alignments [72]. These structural features underly its abilities to adopt pathogenic conformations and its enhanced *in vivo* aggregation kinetics compared to wild-type Aβ [87]. In SCs, overexpressing UAS-Arctic drives a distinctive 'MFAS-organising' activity, producing tightly arranged MFAS aggregates in DCGs that adopt a "dense core"

circular morphology [51, 88] mirroring pathological plaque assemblies observed in human Alzheimer's disease brains (**Figure 6**). This result suggests that Aβ-Arctic can not only organise its own aggregation but can also influence the aggregation of other proteins involved in DCG biogenesis. Post-mating analysis of AGs reveals aggregates reveals GFP-MFAS released from these DCG compartments exhibit a unique lysosomal retention phenotype in MCs (**Figures 19, 20B**). Unlike wild-type and other Aβ mutants that form different fibrillar aggregate morphologies, Aβ-Arctic-induced MFAS-positive structures persist within lysosomal compartments immediately after mating, indicating that these stable MFAS-positive lysosomal structures are resistant to ejection.

Aβ-Iowa and Aβ-Dutch mutations produce amorphous, cloud like plaques resembling those in non-Aβ cerebral amyloidosis [89]. In SCs, these mutants disrupt DCG biogenesis, generating fragmented "mini cores" and non-functional acidified DCGs that are aberrantly released into the gland lumen and are abnormally endocytosed by vulnerable MCs [51]. Aβ-Iowa-induced GFP-MFAS-positive structures within these lysosomes are ejected upon mating, but these abnormal structures appear re-form rapidly (**Figures 19, 20B**). This may reflect Aβ-Iowa's dynamic aggregation kinetics and rapid ability to assemble dense networks of fibrillar bundles [73, 87], although in this case, the mutant peptide is affecting the properties of other secreted proteins, as evidenced by the behaviour of GFP-MFAS. However, Aβ-Dutch (APP E693Q; $A\beta_{42}$ E22Q) displays a different MFAS behaviour profile. It shows an inconsistent abnormal uptake phenotype within MCs and an inability to rapidly re-form post-mating (**Figure 19**). This potentially correlates with its slower aggregation kinetics, producing elongated fibril chains [87]. Interestingly, Aβ-Dutch gives a stronger disrupted DCG phenotype than Aβ-Iowa in SC compartments [51] .

This highlights how single-point mutations localized in the central regions of the Aβ peptide can result in distinct SC and MC phenotypes, affecting the properties of GFP-MFAS secretions, and generating distinct patterns of re-endocytosis and retention within MC lysosomes – mirroring their mutant pathologies in human AD patients [69, 76, 89].

The association between Aβ and secretory/endosomal biology is drawing increasing research activity as intracellular Aβ has gained recognition as a key driver of early neuropathological changes [90]. Work pioneered by the Wilson Group has demonstrated that Aβ mutants disrupt dense-core granule (DCG) formation, leading to abnormal secretory output and altered uptake by neighbouring cells [51].

Notably, this mutant material differs from that of non-mutants, supporting the previous notion that SCs may compensate for trafficking defects of this kind by upregulating trafficking and/or shifting the transfer dynamics to favour the recycling endosomal pathway -- a common feature in patients with AD and other diseases [51, 62]. Notably, the effects of these mutants differ from that of wild type Aβ. Wild type and mutant Aβ all stimulate increased secretion, but presumably the secreted material from mutant-expressing SCs has different properties to wild type-expressing SCs. Interestingly, recent data suggest that wild type Aβ-expressing cells induce DCG defects and a propagation phenotype after 12 days of expression (revision of [51]), indicating that this molecule can induce AD-relevant phenotypes, but on a slower timescale.

The ability of intra-$A\beta_{42}$ mutations (Arctic, Dutch and Iowa), to reorganize MFAS into distinct pathological patterns affecting their secretions properties has led to the latter investigation, to search for the mechanisms that might mediate this transfer [51]. Specifically, I investigated the role of exosomes as intercellular vehicles for amyloidogenic proteins in neurodegenerative disease progression and the interplay between APPL and exosomes at the limiting membranes of DCG compartments.

4.3. Rab11-exosomes from SCs are required to drive the endolysosomal pathology in MCs induced by abnormal membrane-protein aggregate interactions

Exosomes play a dual role in cell-cell communication, both propagating pathological signals and facilitating the clearance of pathogens or toxic aggregates [91]. In SCs, Rab11-exosomes are secreted through the regulated secretory pathway and not via the late endosomal route [62, 63]. Although Rab11-exosomes can represent a small proportion of total extracellular vesicle (EV) secretion, their selective inhibition disrupts both physiological and pathological cell-cell communication [62].

To investigate the role of SC secretion in spreading the APPL-sdΔE1-dependent endolysosomal phenotype in MCs, I both knocked down *Dpp* and overexpressed its transcriptional repressor DAD, both shown to disrupt DCG growth and secretion [59], modulating the amount and composition of secreted SC-derived SFPs within the seminal proteome and impairing several post-mating responses in females [92]. My results showed that as expected, these manipulations significantly reduced the levels of GFP-MFAS in the lumen of the AG (**Figure 21**) and also reduced abnormal transfer of the GFP-MFAS into MCs (**Figure 21**). This suggests that this material is taken up from the luminal content of the AG, which includes SC secretions.

Since non-cleavable APPL and Aβ phenotypes in SCs involve enhanced membrane interactions with DCG aggregates, I hypothesized that Rab11-exosomes themselves might mediate this abnormal secretion phenotype. Initially, I investigated whether GAPDH might be involved, as it is highly concentrated on the surface of EVs, including on Rab11-exosomes, regulating their clustering. GAPDH2 is critical for the coalescence of the SC central DCG [62, 78], and when knocked down, only mini-cores are formed. Despite still colliding, these structures cannot coalesce. This work comes as emerging studies have shown that GAPDH, which is not considered an amyloid protein, is able to interact with Aβ aggregates and accelerate amyloidogenesis [93]. My results indicate that GAPDH2 does not affect the interactions between APPL-sdΔE1 and GFP-MFAS, since it does not facilitate the transfer and uptake of GFP-MFAS by MCs (**Figure 22**).

Importantly, Rab11 has been implicated in Aβ production in late-onset Alzheimer's disease (AD) patients, reinforcing the link between Rab11-mediated trafficking and AD pathology [39]. Studies in *Drosophila* have demonstrated that *Rab11* loss-of-function mutations suppress AD-related phenotypes by diverting APP (which colocalizes with BACE1) toward degradation pathways, thereby inhibiting pathological cargo trafficking [94]. To further dissect the role of Rab11-exosomes in this process, I knocked down *Chmp5*, an accessory Endosomal Sorting Complex Required for Transport (ESCRT-III) component essential for Rab11-exosome biogenesis [63]. My findings reveal that *Chmp5* knockdown in SCs blocks the increased intercellular transfer of GFP-MFAS induced by APPL-sdΔE1 expression, without affecting SC GFP-MFAS secretion (**Figure 22**).

These findings suggest that Rab11-exosomes play a critical role in controlling the levels of endocytosed secreted proteins from SC compartments in which the interactions between membranes and DCG aggregates are enhanced. In preliminary experiments, I found that *Chmp5* knockdown also reduced endocytic uptake of GFP-MFAS in otherwise normal SCs, indicating that this reflects a normal physiological mechanism which is exacerbated when membrane:aggregate dissociation in DCG compartments is suppressed. Importantly, Aβ, which also suppresses membrane:aggregate dissociation in SC DCG compartments, is reported to be complexed with exosomes when released from neurons, and it has been suggested that these exosomes may be important in Aβ-uptake. My work therefore proposes that these Aβ-interacting exosomes may be Rab11-exosomes, and that these potentially pathological effects reflect enhancement of a physiological mechanism involved in some forms of regulated secretion.

4.4 The use of SCs, its future directions and limitations as a model to study regulated secretion and its dys-regulation in Alzheimer's disease

Previous work using the SC-model has established that DCG biogenesis requires transmembrane APPL and proteolytic cleavage to release its extracellular domain. When this

cleavage is impaired, APPL expression is suppressed, or humanized $A\beta_{42}$ mutant peptides are expressed in SCs, DCG biogenesis is disrupted, resulting in the accumulation of acidified, abnormal compartments which are aberrantly secreted. The defectively packaged DCG components are endocytosed by neighbouring MCs located in the AG lobes and accumulate inappropriately in lysosomes, which become highly enlarged and cannot break down the these SC secretions, or at least, GFP-MFAS, a major component of the DCG [51].

In this project, I demonstrate that the abnormal endocytic-uptake phenotype extends beyond the apical tip of the gland where the SCs are located and is distributed through the whole AG body (**Figure 23**). Moreover, once internalized, in glands where SCs express different Aβ-peptides, GFP-MFAS-aggregates appear to reflect some of the discreet molecular properties of each human Aβ mutant in terms of their conformational and aggregation kinetics. My findings suggest that expressing mutant APPL proteins or Aβ-peptides in SCs either increases the levels of endocytosis by MCs and/or affects the ability of MCs to degrade this endocytosed material so that more GFP-MFAS persists and the lysosomes of MCs become acidified and expand.

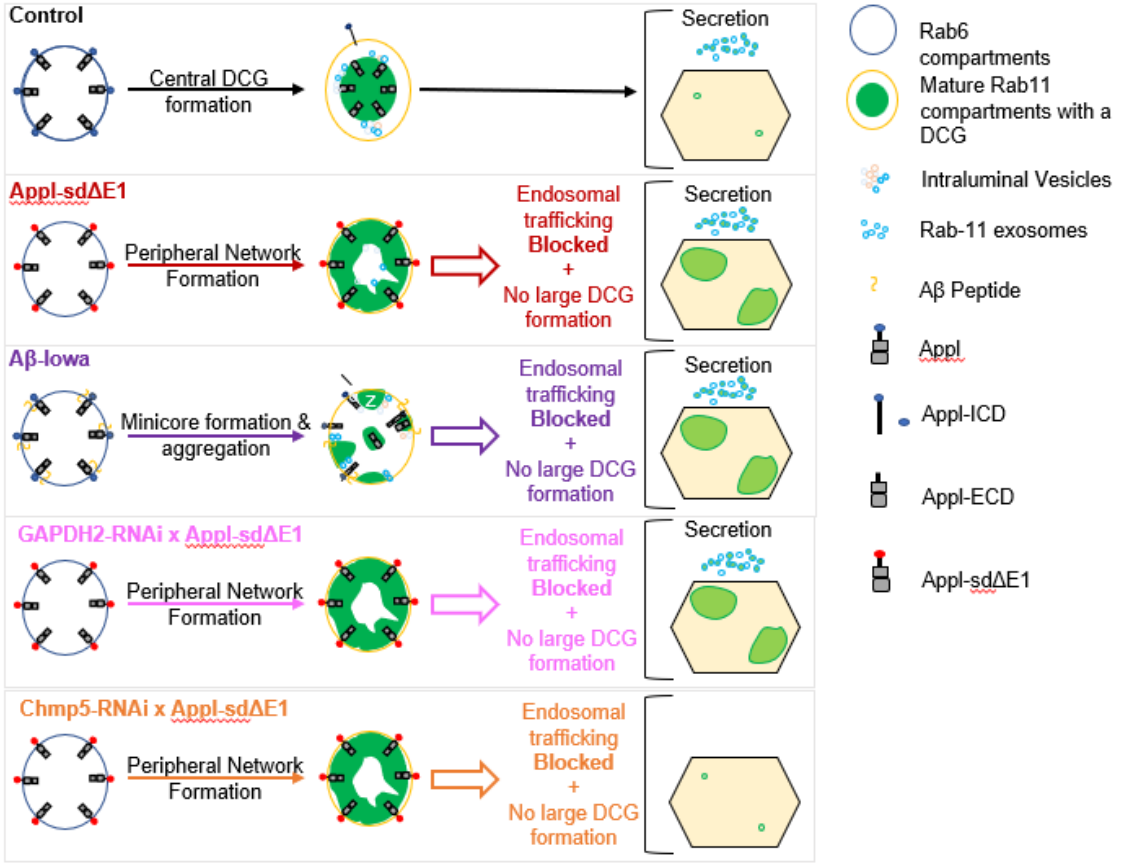

Figure 23. Schematic of model of APPL-regulated DCG formation and secretion into *Drosophila* main cells.

Schematic overviewing my results. It shows central DCG formation in control conditions, in which a large central DCG (green) forms by the condensation of a cloud of diffuse MFAS, often via a peripheral mini-core intermediate stage. This step is triggered by a Rab6 to Rab11 transition. APPL-sdΔE1 mutant expression disrupts DCG assembly and enables MFAS to remain attached to APPL's ECD domain aggregating along the compartment's periphery. Pathological $A\beta_{42}$-Iowa expression disrupts DCG assembly, forming mini cores which remain associated with the compartment's limiting membrane and peripheral ILVs. GAPDH2-RNAi expression also produces a mini-core phenotype, though these mini-cores are motile but fail to fuse when they collide [63]. Expression blocks RAB11-ILV formation but does not have a strong effect on DCG biogenesis. When combined with APPL-sdΔE1, only *Chmp5-RNAi* suppresses the GFP-MFAS endocytic uptake phenotype in MCs induced by this APPL mutant, suggesting that Rab11-exosomes are involved in this process. Figure adapted from [51].

However, several questions remain to be answered, such as how could the properties of mutant APPL or Aβ affect the processing of GFP-MFAS in MCs? Is the effect on GFP-MFAS indirect, primarily reflecting the ability of these mutant molecules to disrupt the MC's endolysosomal system? Or, have the properties of GFP-MFAS itself been altered, so that this molecule contributes to the phenotype? What components of the secretome contribute to this

abnormal endocytic phenotype? The transgenic APPL-sdΔE1 line created by Dr. Bhavna Verma has enabled me to dissect aspects of the molecular mechanisms driving the phenotype. I identified that Chmp5, an essential regulator of Rab11-exosome production, is critical for generating the endolysosomal defects in MCs as scored by GFP-MFAS accumulation, even though it has no obvious effect on SC secretion of GFP-MFAS itself.

Moving forward, it will be important to screen other AD-risk genes using the SC model to identify other potential factors governing DCG biogenesis in SCs and the endocytic processing of secreted material by MCs, which may have broader relevance to AD pathology. For example, currently Wilson lab members are leveraging this system to investigate the role of insulin-related genes in regulating DCG biogenesis and quality control.

In addition, I initially utilised the *Drosophila* female reproductive tract to assay the uptake dynamics of MFAS following mating. In this system, MFAS is transferred into the uterus where it is retained in the lumen for up to three hours post-mating before being expelled during egg-laying. Initial data has shown that prior to ejection the seminal-MFAS coagulum may be degraded by seminal proteases at distinct rates, as monomeric Aβ-WT-containing fluid degraded rapidly in comparison with Arctic and Iowa, whose proteolysis has been shown to be less efficient in studies. This would suggest that the properties of Aβ-peptides can affect other molecules such as GFP-MFAS, arguing that these molecules interact even after secretion or that mutant Aβ blocks protease activity. Potentially, by mating $A\beta_{42}$ mutants with mutant females that prevent egg laying, we may be able to further view degradative dynamics [95]. This model has the potential to not only expand our knowledge of $A\beta_{42}$-mediated pathological effects, but also to improve our understanding of how these peptides interact and influence the behaviours of other proteins.

Furthermore, we can utilise the SC-system as a model to study the molecular mechanisms of Rab11-exosome-mediated phenotype propagation and its associated endolysosomal defects. By using using this approach, we can investigate whether other fAD-mutants, particularly

those that resemble specific aspects of sporadic AD pathology [76], and Tau isoforms that have shown promote propagation in AGs [private communication] can be supressed in a similar way to APPL-sdΔE1 pathology. I believe this further work has the potential to establish the SC-model as a high throughput assay to investigate AD-mutants and their conserved pathways of EV-mediated amyloid spread.

4.4.1 Limitations

Although this model provides a promising foundation for future studies, several limitations remain within the experimental procedures presented in this work. As this thesis primarily serves as a proof of concept rather than a comprehensive quantitative analysis, further experimental replicates are required to strengthen the validity and reproducibility of these finding. This is especially important for the mating experiments, which currently include only six biological repeats.

Furthermore, adopting a computational image-analysis approach utilising machine learning (ML) methodologies could help address these underlying limitations by reducing human bias and enhancing the objectivity of image quantification. In particular, AI programmes such as ComPRePS, have been shown to capture and quantify subtle patterns in pathology similar to those observed in this model [96]. By implementing these approaches, this model has the potential to develop an automated and unbiased analytical database that will facilitate a more rigorous and scalable investigation of secretion dynamics and Alzheimer's disease–related pathology.

4.5 Conclusions

In conclusion, expression of non-cleavable APPL-sdΔE1 and amyloidogenic Aβ42 mutants, which disrupt dense-core granule (DCG) biogenesis drive the aberrant uptake and

endolysosomal processing of secreted proteins within specific populations of MCs - potentially mirroring the propagation phenotype observed in AD progression. Furthermore, these fAD mutants reorganise the properties of secreted GFP-MFAS MFAS in patterns that reflect the discreet aspects of the molecular architecture characteristic of human AD plaque pathology, which remain challenging to model in conventional or iPSC-based systems.

Critically, I demonstrate that transfer of the APPL-sdΔE1;MFAS phenotype specific subset of exosomes, termed Rab11-positive exosomes which are formed in the same secretory compartments where they interact with DCG aggregates in normal SCs. Thus, this SC-cell based model can potentially provide a versatile platform to systematically interrogate AD risk genes and identify therapeutic strategies targeting amyloid spread by leveraging its dependence on Rab11-exosomes.

References

1. *Review: History of the Amyloid Fibril.* Journal of Structural Biology, 2000/06/01. **130**(2-3).
2. Del Pozo-Yauner, L., et al., *The Structural Determinants of the Immunoglobulin Light Chain Amyloid.* Physical Biology of Proteins and Peptides, 2015.
3. Astbury, W.T., S. Dickinson, and K. Bailey, *The X-ray interpretation of denaturation and the structure of the seed globulins.* Biochemical Journal, 1935/10. **29**(10).
4. *A crystal-structural study of Pauling–Corey rippled sheets.* Chemical Science, 2022/01/19. **13**(3).
5. Raskatov, J.A., J.P. Schneider, and B.L. Nilsson, *Defining the Landscape of the Pauling-Corey Rippled Sheet: An Orphaned Motif Finding New Homes.* Accounts of Chemical Research, April 26, 2021. **54**(10).
6. *Metabolite amyloids: a new paradigm for inborn error of metabolism disorders - PubMed.* Journal of inherited metabolic disease, 2016 Jul. **39**(4).
7. B, L., *Rippled Sheets: The Early Polyglycine Days and Recent Developments in Nylons - PubMed.* Chembiochem : a European journal of chemical biology, 03/04/2022. **23**(5).
8. Hruby, V.J. and D. Patel, *Structure–Function Studies of Peptide Hormones: An Overview.* Peptides, 1995/01/01.
9. Hurbain, I., et al., *Electron tomography of early melanosomes: Implications for melanogenesis and the generation of fibrillar amyloid sheets.* Proceedings of the National Academy of Sciences of the United States of America, 2008/12/12. **105**(50).
10. Otzen, D. and R. Riek, *Functional Amyloids.* Cold Spring Harbor Perspectives in Biology, 2019/12. **11**(12).
11. A, K., et al., *Peptidoglycan-Sensing Receptors Trigger the Formation of Functional Amyloids of the Adaptor Protein Imd to Initiate Drosophila NF-κB Signaling - PubMed.* Immunity, 10/17/2017. **47**(4).
12. *Semen amyloids participate in spermatozoa selection and clearance.* 2017-06-27.
13. *Functional Amyloids: Where Supramolecular Amyloid Assembly Controls Biological Activity or Generates New Functionality.* Journal of Molecular Biology, 2023/06/01. **435**(11).
14. *Functional amyloids in the human body.* Bioorganic & Medicinal Chemistry Letters, 2021/05/15. **40**.
15. DeTure, M.A., et al., *The neuropathological diagnosis of Alzheimer's disease.* Molecular Neurodegeneration 2019 14:1, 2019-08-02. **14**(1).
16. *Global estimates on the number of persons across the Alzheimer's disease continuum - PubMed.* Alzheimer's & dementia : the journal of the Alzheimer's Association, 2023 Feb. **19**(2).
17. Török, M. and M. Török, *Amyloids in synthetic applications.* Scientific Reports 2022 12:1, 2022-12-08. **12**(1).
18. GS, B., *Amyloid-β and tau: the trigger and bullet in Alzheimer disease pathogenesis - PubMed.* JAMA neurology, 2014 Apr. **71**(4).
19. *Alzheimer's Disease: The Amyloid Cascade Hypothesis.* Science, 1992. **256**(5054).
20. Barmaki, H., A. Nourazarian, and F. Khaki-Khatibi, *Proteostasis and neurodegeneration: a closer look at autophagy in Alzheimer's disease.* Frontiers in Aging Neuroscience, 2023 Nov 2. **15**.
21. DR, T., et al., *Phases of A beta-deposition in the human brain and its relevance for the development of AD - PubMed.* Neurology, 06/25/2002. **58**(12).
22. MJ, G., et al., *In vivo staging of regional amyloid deposition - PubMed.* Neurology, 11/14/2017. **89**(20).
23. Swarbrick, S., et al., *Systematic Review of miRNA as Biomarkers in Alzheimer's Disease.* Molecular Neurobiology 2019 56:9, 2019-02-08. **56**(9).
24. R, C., et al., *Role of Amyloid Precursor Protein (APP) and Its Derivatives in the Biology and Cell Fate Specification of Neural Stem Cells - PubMed.* Molecular neurobiology, 2018 Sep. **55**(9).
25. Puig, K.L. and C.K. Combs, *Expression and Function of APP and its Metabolites Outside the Central Nervous System.* Experimental gerontology, 2012 Jul 27. **48**(7).
26. RJ, A., et al., *A Greek Tragedy: The Growing Complexity of Alzheimer Amyloid Precursor Protein Proteolysis - PubMed.* The Journal of biological chemistry, 09/09/2016. **291**(37).

27. Chen, G.-f., et al., *Amyloid beta: structure, biology and structure-based therapeutic development.* Acta Pharmacologica Sinica 2017 38:9, 2017-07-17. **38**(9).
28. Yang, M. and D.B. Teplow, *Amyloid β-protein monomer folding: free energy surfaces reveal alloform specific differences.* Journal of molecular biology, 2008 Sep 24. **384**(2).
29. Hampel, H., et al., *The Amyloid-β Pathway in Alzheimer's Disease.* Molecular Psychiatry 2021 26:10, 2021-08-30. **26**(10).
30. Schilling, S., et al., *Differential effects of familial Alzheimer's disease-causing mutations on amyloid precursor protein (APP) trafficking, proteolytic conversion, and synaptogenic activity.* Acta Neuropathologica Communications 2023 11:1, 2023-06-01. **11**(1).
31. WE, V.N., et al., *Pathogenic effects of cerebral amyloid angiopathy mutations in the amyloid beta-protein precursor - PubMed.* Annals of the New York Academy of Sciences, 2002 Nov. **977**(1).
32. Rensink, A.A.M., et al., *Pathogenesis of cerebral amyloid angiopathy.* Brain Research Reviews, 2003/10/01. **43**(2).
33. Sahlin, C., et al., *The Arctic Alzheimer mutation favors intracellular amyloid-β production by making amyloid precursor protein less available to α-secretase.* Journal of Neurochemistry, 2007/05/01. **101**(3).
34. Knobloch, M., et al., *Intracellular Aβ and cognitive deficits precede β-amyloid deposition in transgenic arcAβ mice.* Neurobiology of Aging, 2007/09/01. **28**(9).
35. Cataldo, A.M., et al., *Endocytic Pathway Abnormalities Precede Amyloid β Deposition in Sporadic Alzheimer's Disease and Down Syndrome: Differential Effects of APOE Genotype and Presenilin Mutations.* The American Journal of Pathology, 2000/07/01. **157**(1).
36. Konings, S.C., et al., *Apolipoprotein E intersects with amyloid-β within neurons.* Life Science Alliance, 2023-08-01. **6**(8).
37. Zhang, J., Z. Jiang, and A. Shi, *Rab GTPases: The principal players in crafting the regulatory landscape of endosomal trafficking.* Computational and Structural Biotechnology Journal, 2022 Aug 11. **20**.
38. Grbovic, O.M., et al., *Rab5-stimulated Up-regulation of the Endocytic Pathway Increases Intracellular β-Cleaved Amyloid Precursor Protein Carboxyl-terminal Fragment Levels and Aβ Production.* Journal of Biological Chemistry, 2003/08/15. **278**(33).
39. Udayar, V., et al., *A Paired RNAi and RabGAP Overexpression Screen Identifies Rab11 as a Regulator of β-Amyloid Production.* Cell reports, 2013 Dec 26. **5**(6).
40. Small, S.A. and G.A. Petsko, *Endosomal Recycling Reconciles the Alzheimer's Paradox.* Science translational medicine, 2020 Dec 2. **12**(572).
41. CM, K. and G. AM, *Alzheimer's disease risk genes and mechanisms of disease pathogenesis - PubMed.* Biological psychiatry, 01/01/2015. **77**(1).
42. Bhattacharyya, R., et al., *The neuronal-specific isoform of BIN1 regulates β-secretase cleavage of APP and Aβ generation in a RIN3-dependent manner.* Scientific Reports, 2022 Mar 3. **12**(1).
43. Müller, U.C. and H. Zheng, *Physiological Functions of APP Family Proteins.* Cold Spring Harbor Perspectives in Medicine, 2012 Feb. **2**(2).
44. Carmine-Simmen, K., et al., *Neurotoxic effects induced by the Drosophila amyloid-β peptide suggest a conserved toxic function.* Neurobiology of disease, 2008 Nov 8. **33**(2).
45. Luo, L., T. Tully, and K. White, *Human amyloid precursor protein ameliorates behavioral deficit of flies deleted for appl gene.* Neuron, 1992/10/01. **9**(4).
46. V, N., et al., *Integrative analysis reveals a conserved role for the amyloid precursor protein in proteostasis during aging - PubMed.* Nature communications, 11/03/2023. **14**(1).
47. Rodrigue, K.M., et al., *Beta-Amyloid Deposition and the Aging Brain.* Neuropsychology Review 2009 19:4, 2009-11-12. **19**(4).
48. Z, M., et al., *Drosophila melanogaster: A Model Organism to Study Cancer - PubMed.* Frontiers in genetics, 03/01/2019. **10**.
49. Shih, J., R. Hodge, and M.A. Andrade-Navarro, *Comparison of inter- and intraspecies variation in humans and fruit flies.* Genomics Data, 2015/03/01. **3**.
50. SE, M., et al., *Spatiotemporal rescue of memory dysfunction in Drosophila - PubMed.* Science (New York, N.Y.), 12/05/2003. **302**(5651).
51. Singh, P.J., et al., *APP and β-amyloid modulate protein aggregation and dissociation from recycling endosomal and exosomal membranes.* bioRxiv, 2024-03-30.
52. Wilson, C., et al., *Chapter Eleven: The Drosophila Accessory Gland as a Model for Prostate Cancer and Other Pathologies.* Current topics in developmental biology, 2017. **121**.
53. *Cell type-specific gene expression in the Drosophila melanogaster male accessory gland - PubMed.* Mechanisms of development, 1992 Jul. **38**(1).

54. Kubo, A., et al., *Nutrient conditions sensed by the reproductive organ during development optimize male fecundity in Drosophila.* Genes to Cells, 2018/07/01. **23**(7).
55. PS, C., et al., *A male accessory gland peptide that regulates reproductive behavior of female D. melanogaster - PubMed.* Cell, 07/29/1988. **54**(3).
56. Kalb, J.M., A.J. DiBenedetto, and M.F. Wolfner, *Probing the function of Drosophila melanogaster accessory glands by directed cell ablation.* Proceedings of the National Academy of Sciences of the United States of America, 1993 Sep 1. **90**(17).
57. E, K. and B. D, *Sexual behavior: how Sex Peptide flips the postmating switch of female flies - PubMed.* Current biology : CB, 07/10/2012. **22**(13).
58. JL, S., et al., *The Female Post-Mating Response Requires Genes Expressed in the Secondary Cells of the Male Accessory Gland in Drosophila melanogaster - PubMed.* Genetics, 2016 Mar. **202**(3).
59. Redhai, S., et al., *Regulation of Dense-Core Granule Replenishment by Autocrine BMP Signalling in Drosophila Secondary Cells.* PLoS Genetics, 2016/10. **12**(10).
60. L, C., et al., *BMP-regulated exosomes from Drosophila male reproductive glands reprogram female behavior - PubMed.* The Journal of cell biology, 09/01/2014. **206**(5).
61. Wells, A., et al., *A Rab6 to Rab11 transition is required for dense-core granule and exosome biogenesis in Drosophila secondary cells.* PLOS Genetics, 2023 Oct 16. **19**(10).
62. Fan, S.J., et al., *Glutamine deprivation alters the origin and function of cancer cell exosomes.* The EMBO Journal, 2020-07-28. **39**(16).
63. Marie, P.P., et al., *Accessory ESCRT-III proteins are conserved and selective regulators of Rab11a-exosome formation.* Journal of Extracellular Vesicles, 2023 Mar 5. **12**(3).
64. Laurent, P., et al., *Genetic dissection of neuropeptide cell biology at high and low activity in a defined sensory neuron.* Proceedings of the National Academy of Sciences of the United States of America, 2018 Jun 29. **115**(29).
65. A, S., et al., *ARF1 compartments direct cargo flow via maturation into recycling endosomes - PubMed.* Nature cell biology, 2024 Nov. **26**(11).
66. Wainwright, S.M., et al., *Drosophila Sex Peptide controls the assembly of lipid microcarriers in seminal fluid.* Proceedings of the National Academy of Sciences, 2021-02-02. **118**(5).
67. Hardy, J.A. and G.A. Higgins, *Alzheimer's Disease: The Amyloid Cascade Hypothesis.* Science, 1992-4-10. **256**(5054).
68. Lu, M., et al., *Structural progression of amyloid-β Arctic mutant aggregation in cells revealed by multiparametric imaging.* The Journal of Biological Chemistry, 2018 Nov 30. **294**(5).
69. *Amyloid β Protein Precursor Gene and Hereditary Cerebral Hemorrhage with Amyloidosis (Dutch).* Science, 1990. **248**(4959).
70. Grabowski, T.J., et al., *Novel amyloid precursor protein mutation in an Iowa family with dementia and severe cerebral amyloid angiopathy.* Annals of Neurology, 2001/06/01. **49**(6).
71. Kim, W. and M.H. Hecht, *Mutations Enhance the Aggregation Propensity of the Alzheimer's Aβ Peptide.* Journal of Molecular Biology, 2008/03/21. **377**(2).
72. Fawzi, N.L., et al., *Protofibril Assemblies of the Arctic, Dutch, and Flemish Mutants of the Alzheimer's Aβ1–40 Peptide.* Biophysical Journal, 2007 Nov 21. **94**(6).
73. Krone, M.G., et al., *Effects of Familial Alzheimer's Disease Mutations on the Folding Nucleation of the Amyloid β-Protein.* Journal of Molecular Biology, 2008/08/01. **381**(1).
74. Fernandez-Funez, P., L.d. Mena, and D.E. Rincon-Limas, *Modeling the complex pathology of Alzheimer's disease in Drosophila.* Experimental neurology, 2015 May 27. **274**(0 0).
75. Iijima, K., et al., *Aβ42 Mutants with Different Aggregation Profiles Induce Distinct Pathologies in Drosophila.* PLoS ONE, 2008 Feb 27. **3**(2).
76. Basun, H., et al., *Clinical and neuropathological features of the Arctic APP mutation causing early onset Alzheimer's disease.* Archives of neurology, 2008 Apr. **65**(4).
77. Ruhmann, H., et al., *Early reproductive success in Drosophila males is dependent on maturity of the accessory gland.* Behavioral Ecology, 2016/11/01. **27**(6).
78. GH, D., et al., *GAPDH controls extracellular vesicle biogenesis and enhances the therapeutic potential of EV mediated siRNA delivery to the brain - PubMed.* Nature communications, 11/18/2021. **12**(1).
79. Kimura, N. and K. Yanagisawa, *Traffic jam hypothesis: Relationship between endocytic dysfunction and Alzheimer's disease.* Neurochemistry International, 2018/10/01. **119**.
80. Noda, Y., et al., *Copper enhances APP dimerization and promotes Aβ production.* Neuroscience Letters, 2013/06/28. **547**.
81. Opazo, C.M., M.A. Greenough, and A.I. Bush, *Frontiers | Copper: from neurotransmission to neuroproteostasis.* Frontiers in Aging Neuroscience, 2014/07/03. **6**.

82. Singh, S.K., et al., *Neuroprotective Role of a Novel Copper Chelator against Aβ 42 Induced Neurotoxicity.* International Journal of Alzheimer's Disease, 2013 Sep 18. **2013**.
83. Hartwig, C., et al., *Golgi-Dependent Copper Homeostasis Sustains Synaptic Development and Mitochondrial Content.* bioRxiv, 2020-05-23.
84. Mathys, H., et al., *Single-cell transcriptomic analysis of Alzheimer's disease.* Nature 2019 570:7761, 2019-05-01. **570**(7761).
85. Mathys, H., et al., *Single-cell multiregion dissection of Alzheimer's disease.* Nature 2024 632:8026, 2024-07-24. **632**(8026).
86. Majane, A.C., J.M. Cridland, and D.J. Begun, *Single-nucleus transcriptomes reveal evolutionary and functional properties of cell types in the Drosophila accessory gland.* Genetics, 2021 Nov 25. **220**(2).
87. Hatami, A., et al., *Familial Alzheimer's Disease Mutations within the Amyloid Precursor Protein Alter the Aggregation and Conformation of the Amyloid-β Peptide.* Journal of Biological Chemistry, 2017/02/24. **292**(8).
88. Singh, P., *The physiological and pathological aggregation of transforming growth factor-β-induced and amyloid precursor protein in drosophila secondary cells*, in *The physiological and pathological aggregation of transforming growth factor-β-induced and amyloid precursor protein in drosophila secondary cells*. 2023.
89. Tomidokoro, Y., et al., *Iowa Variant of Familial Alzheimer's Disease: Accumulation of Posttranslationally Modified AβD23N in Parenchymal and Cerebrovascular Amyloid Deposits.* The American Journal of Pathology, 2010 Apr. **176**(4).
90. Okazawa, H., *Intracellular amyloid hypothesis for ultra-early phase pathology of Alzheimer's disease.* Neuropathology, 2021 Apr 20. **41**(2).
91. Jahangiri, B., et al., *Exosomes, autophagy and ER stress pathways in human diseases: Cross-regulation and therapeutic approaches.* Biochimica et Biophysica Acta (BBA) - Molecular Basis of Disease, 2022/10/01. **1868**(10).
92. Hopkins, B.R., et al., *BMP signaling inhibition in Drosophila secondary cells remodels the seminal proteome and self and rival ejaculate functions.* Proceedings of the National Academy of Sciences of the United States of America, 2019 Nov 18. **116**(49).
93. Lazarev, V.F., et al., *Extracellular GAPDH Promotes Alzheimer Disease Progression by Enhancing Amyloid-β Aggregation and Cytotoxicity.* Aging and Disease, 2021 Aug 1. **12**(5).
94. Walsh, R.B., et al., *Opposing functions for retromer and Rab11 in extracellular vesicle traffic at presynaptic terminals.* The Journal of Cell Biology, 2021 May 21. **220**(8).
95. KM, L., et al., *A neuronal pathway that controls sperm ejection and storage in female Drosophila - PubMed.* Current biology : CB, 03/16/2015. **25**(6).
96. Mimar, S., et al., *ComPRePS: An Automated Cloud-based Image Analysis tool to democratize AI in Digital Pathology.* Proceedings of SPIE--the International Society for Optical Engineering, 2024 Apr 3. **12933**.